Geotechnical Reconnaissance and Engineering Effects of the December 29, 2020, M6.4 Petrinja, Croatia Earthquake, and Associated Seismic Sequence

Chapter 6: Cover-Collapse Sinkholes

Authors: Ingrid Tomac, Igor Vlahović, Jelena Parlov, BojanMatoš, Darko Matešić, Ivan Kosović, Ivica Pavičić, Tihomir Frangen, Josip Terzić, Davor Pavelić, Nguyen Pham

6. Cover-Collapse Sinkholes

6.1 Geological Setting

GEER reconnaissance team registered 91 cover-collapse sinkholes that opened because of the Petrinja earthquake of December 29, 2020, and numerous aftershocks. Sinkholes appeared within the small 4 km^2 area surrounding Mečenčani and Borojevići villages located 20–25 km SE of the epicentral area during only three months. Although the proposed trace of Petrinja fault as a seismogenic source stretches very close, Mečenčani and Borojevići are outside of the most active fault segment: epicenters of only a few low-magnitude earthquakes were near the sinkhole area (**Figure 6.1**). Cover-collapse sinkholes found in Mečenčani and Borojevići formed due to the particular combination of heavily karstified limestones covered by relatively thick clayey soil. Therefore, in the approximately 1.000 km^2 large area affected by the Petrinja earthquake sequence, only a small area of roughly 4 km^2 is prone to cover-collapse sinkholes (**Figures 6.2** and **6.3**). Subhorizontal Badenian deposits (M_4) are composed of alternating highly porous Lithothamnium limestones and calcarenites that are very susceptible to karstification. Karst phenomena form, for example, sinkholes/dolines visible on outcrops in the neighboring hilly area SW of Mečenčani and Borojevići. A 4–15 m thick sequence of Holocene deluvial–proluvialdeposits (dpr) built of clays with interlayers lenses of gravel and sand in lateral and vertical alternations covers the heavily karstified carbonate bedrock.

During wet periods high water pressure from underlying highly permeable confined karst aquifer caused both gradual underground erosion of non-cohesive fine-grained cover soil (suffosion) or successive failures of cohesive soil (see Gutiérrez and Cooper, 2013). Continuous removal of eroded sediment caused by groundwater flow through karstified systems in underlying carbonates creates and gradually expands cavernous space. Unlike subsidence that slowly creates depressions with gentle slopes by suffosion in non-cohesive deposits, the collapse of cover cohesive soil deposits is sudden, usually occurring within minutes or hours. Cover-collapse structures usually have steep or even overhanging margins – as most of the studied in the vicinity of Mečenčani and Borojevići – and occur mostly in more competent rocks. The collapse of cover deposits is more common during periods of heavy rainfall, as water significantly increases the total weight of soil and at the same time reduces soil strength and arching stability.

Mečenčani and Borojevići areas are naturally prone to cover-collapse sinkholes. Therefore, in addition to 91 recently opened sinkholes, a total of 45 **fossil cover-collapse sinkholes** formed before the 2020–2021 Petrinja earthquake series were registered by the GEER team (**Figures 6.2** to **6.5**). Several of these sinkholes were filled up years ago by local farmers and did not reactivate during the studied earthquake series, except for subtle subsidence recorded in a few of them (mostly around 10 cm). Eight out of ten largest sinkholes found in the area are fossil ones, having the largest diameter between 10 and 18 m (including major springs in the area, Davidovića vrelo and Pašino vrelo located close to the Sunja river).

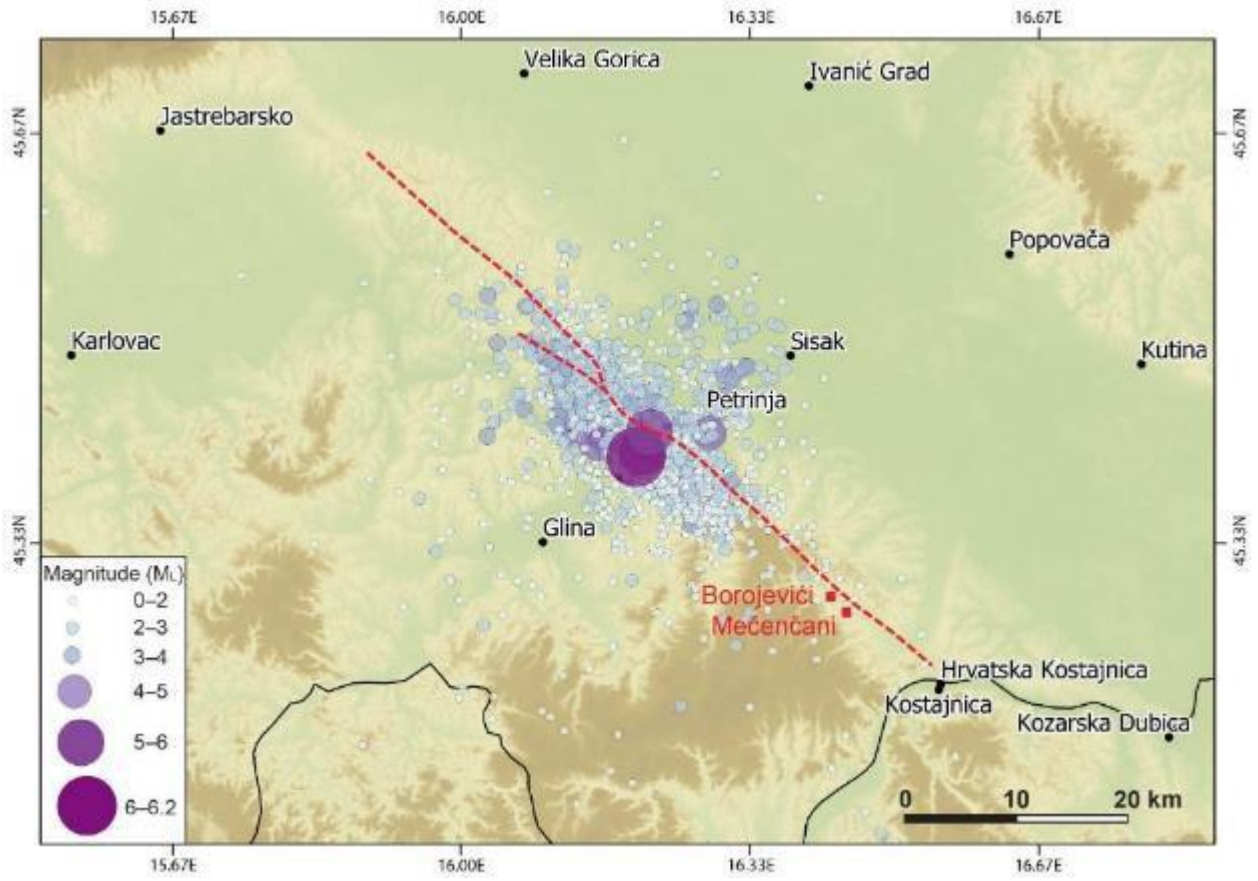

Figure 6.1 Map of the preliminary position of earthquake epicenters in the Petrinja area from December 28, 2020, to January 28, 2021, with approximate fault position estimated with InSAR analysis (Chapter 5) and Borojevići and Mečenčani villages. Note that only a few epicenters of low-magnitude earthquakes are around this area characterized by numerous cover-collapse sinkholes. Map of earthquake epicenters by the Croatian Seismologic Survey (2021)

Fossil sinkholes are generally morphologically very similar to recent ones, including common very steep to sub-vertical walls. However, besides testimonies of local farmers, three major characteristics enabled their recognition:

(1) Lack of freshly opened collapsed margins and irregular cover of fresh soil and grass at their bottoms.

(2) Common old trees are growing, including sometimes old garbage found at their bottoms.

(3) In the case of sinkholes filled with water, fossil sinkholes are characterized by abundant fresh-water macrophytic vegetation, while newly formed sinkholes have no fresh-water plants.

Numerous earthquakes significantly accelerated natural processes in the area: according to local people, a new cover-collapse sinkhole would be opened in the area once every few years. The changes in stress states caused by the 2020–2021 Petrinja Earthquake Sequence resulted in the opening of as many as 91 cover-collapse sinkholes within only three months. We speculate that

high groundwater levels additionally fostered such an intense sinkhole collapsing during Petrinja Earthquake Sequence during the studied period.

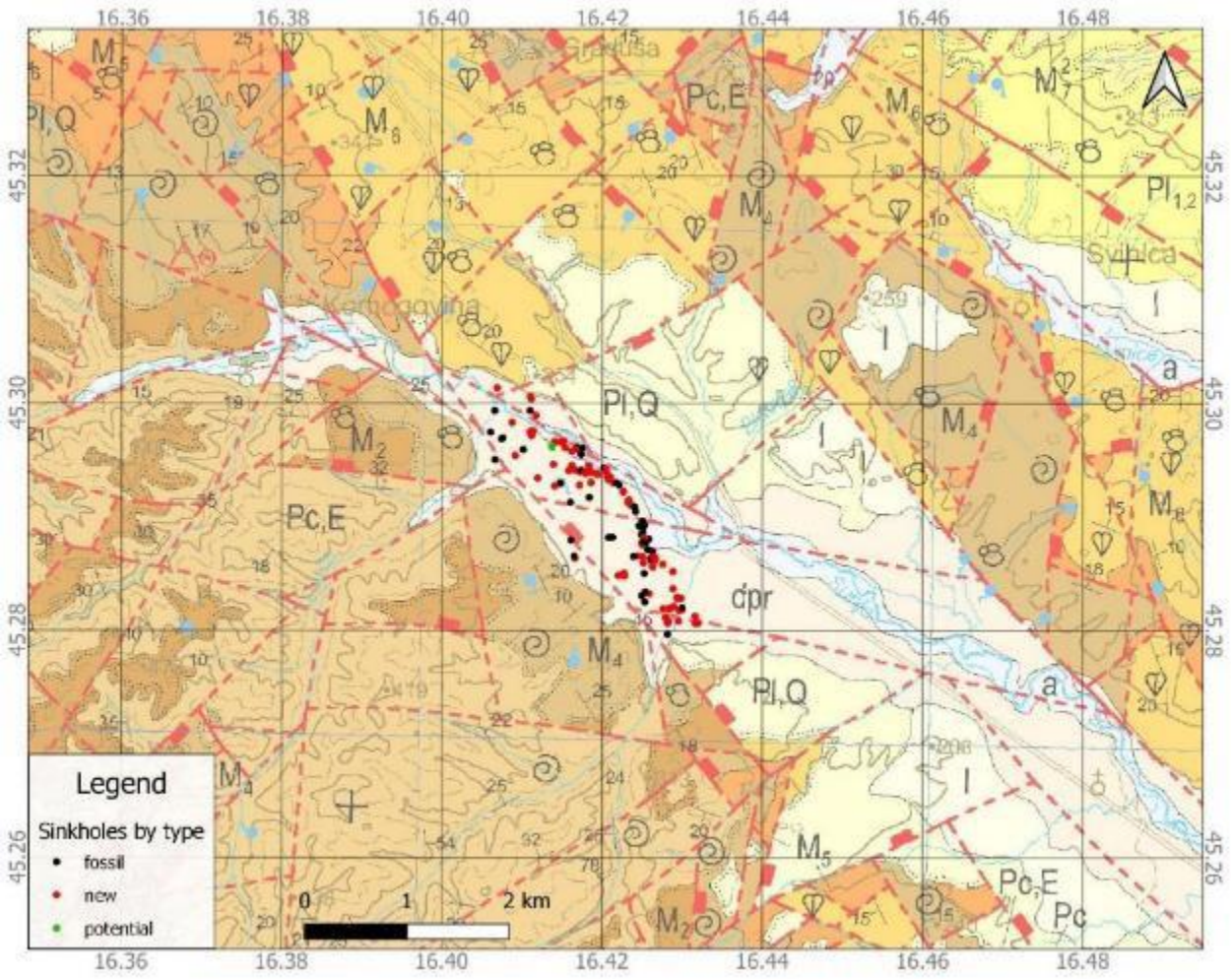

Figure 6.2. Detail of the Basic geological map of the Republic of Croatia 1:100,000, Bosanski Novi sheet (Šikić, 2014) with the position of studied cover-collapse sinkholes. Note that all sinkholes are in the small area where deluvial–proluvial deposits (dpr) cover Middle Miocene limestones and calcarenites (M_4, Badenian).

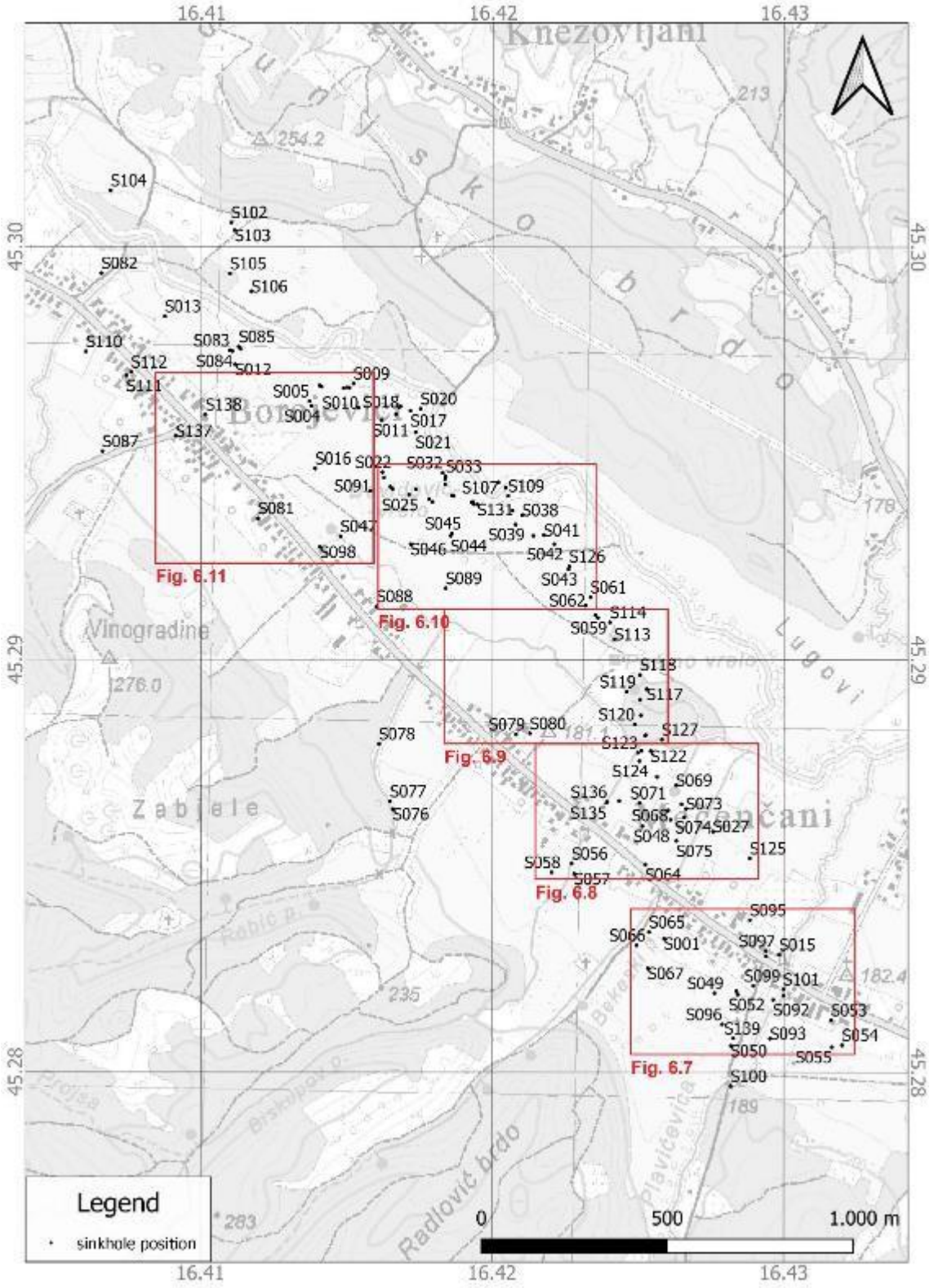

Figure 6.3 Position of cover-collapse sinkholes in Borojevići and Mečenčani on the topographic map with positions of areal photogrammetry shown in **Figures 6.7** to **6.11**.

Figure 6.4 Sinkhole S069, with the largest diameter of 16.8 m, is a fossil cover-collapse sinkhole representing a freshwater spring (45.28696N, 16.42630E).

6.2 Spatio-Temporal Dynamics of Earthquake-Induced Cover-Collapse Sinkholes in Mečenčani–Borojevići area

Local and virtual reconnaissance teams recovered and assembled spatio-temporal data from drone imaging, field observations, and critical consideration of multiple interviews with residents and police. Although residents provided new sinkholes positions, information about their opening time was often inaccurate and confusing. During the first month after the major earthquake, drones flew exclusively by the Croatian Mountain Rescue Service (HGSS), followed by four drone campaigns by the GEER team members. Three drone flights were by the Croatian Geological Survey on January 29, March 4, and March 31, and one by the Faculty of Mining, Geology and Petroleum Engineering on February 18 and 19.

Figure 6.5 shows spatio-temporal positions of sinkholes sorted into time windows of appearance and sizes. The GEER team could not obtain better resolution data than the time windows presented in **Figure 6.5**. Grey-colored circles represent fossil sinkholes, which are pre-existing cover-collapse sinkholes. A more significant number of fossil sinkholes characterize the area between two villages, including Pašino vrelo (vrelo meaning spring in Croatian). Pašino vrelo has been turned into a commercial well and serves as a drinking water source for Hrvatska Kostajnica. Fewer but relatively larger and deeper sinkholes and fewer of them per area collapsed in the eastern part around Mečenčani than in the north of Borojevići. The biggest sinkhole, 25x23 m in

diameter and 11.7 m deep, is in Mečenčani and the second-largest new sinkhole, 10.8x9.8 m in diameter and 3.6 m deep.

A total of 136 cover-collapse sinkholes (45 fossil and 91 newly opened), as well as three potential sinkholes were observed and documented. Lengths, widths, and depths were measured directly on-site for each sinkhole, and lidar point clouds were collected for 63 sinkholes and are curated in NHERI NSF DesignSafe Data Depot. The majority of sinkholes appeared dry during the reconnaissance, while some also had standing water. Depths of sinkholes and time of appearance are shown in **Figure 6.6**. Areal images of drone flights acquired by the Croatian Geological Survey show parts of the area in **Figures 6.7 to 6.11**. The GEER team identified the fossil in black circles and new, in white circles, cover-collapse sinkholes. The largest sinkhole is shown in **Figure 6.7** as S001, Pašino vrelo pumping station is in Figure 6.6 between S113 and S118.

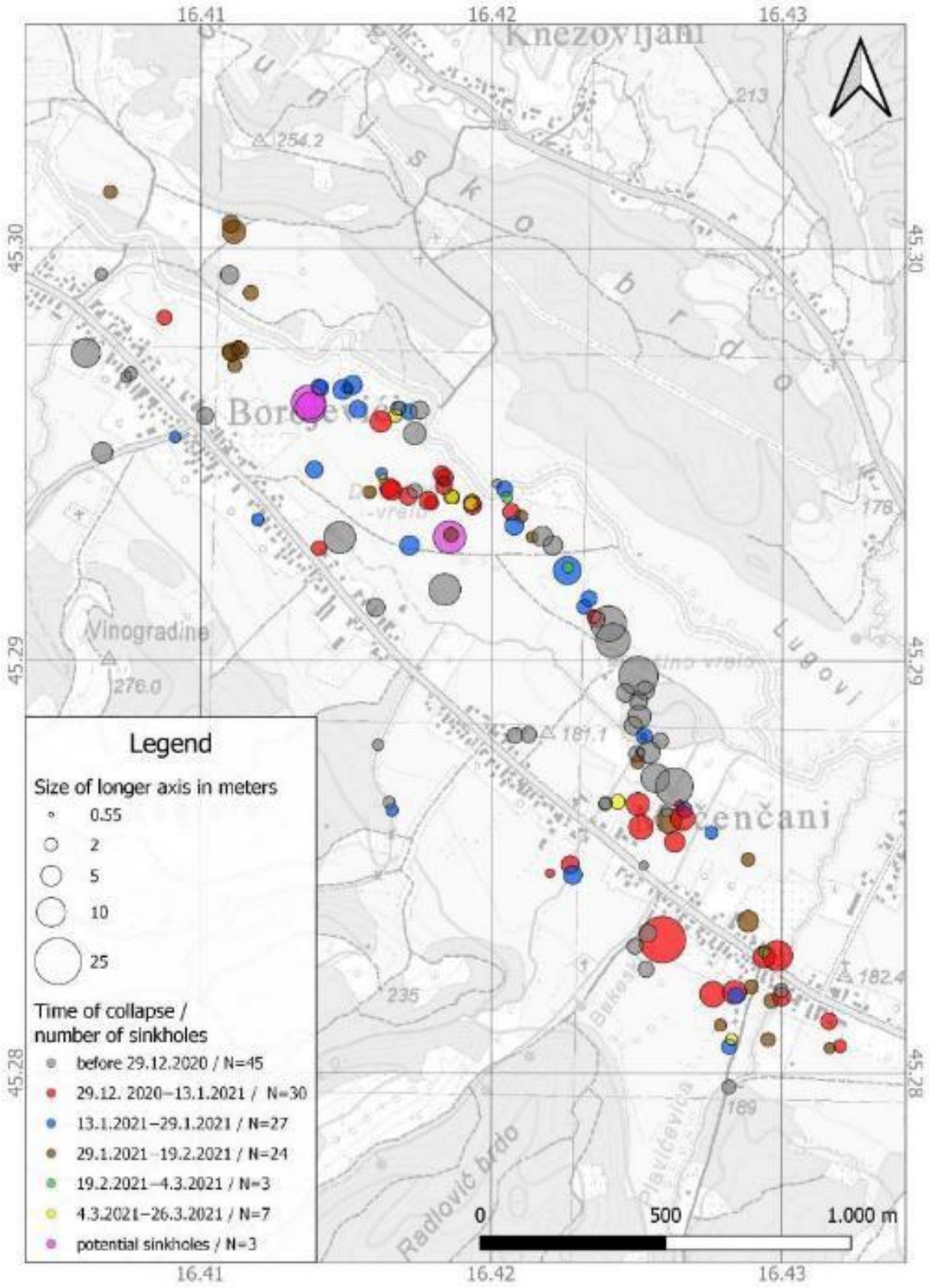

Figure 6.5 Spatio-temporal map of sinkholes in Borojevići and Mečenčani and their longer diameter on the topographic map.

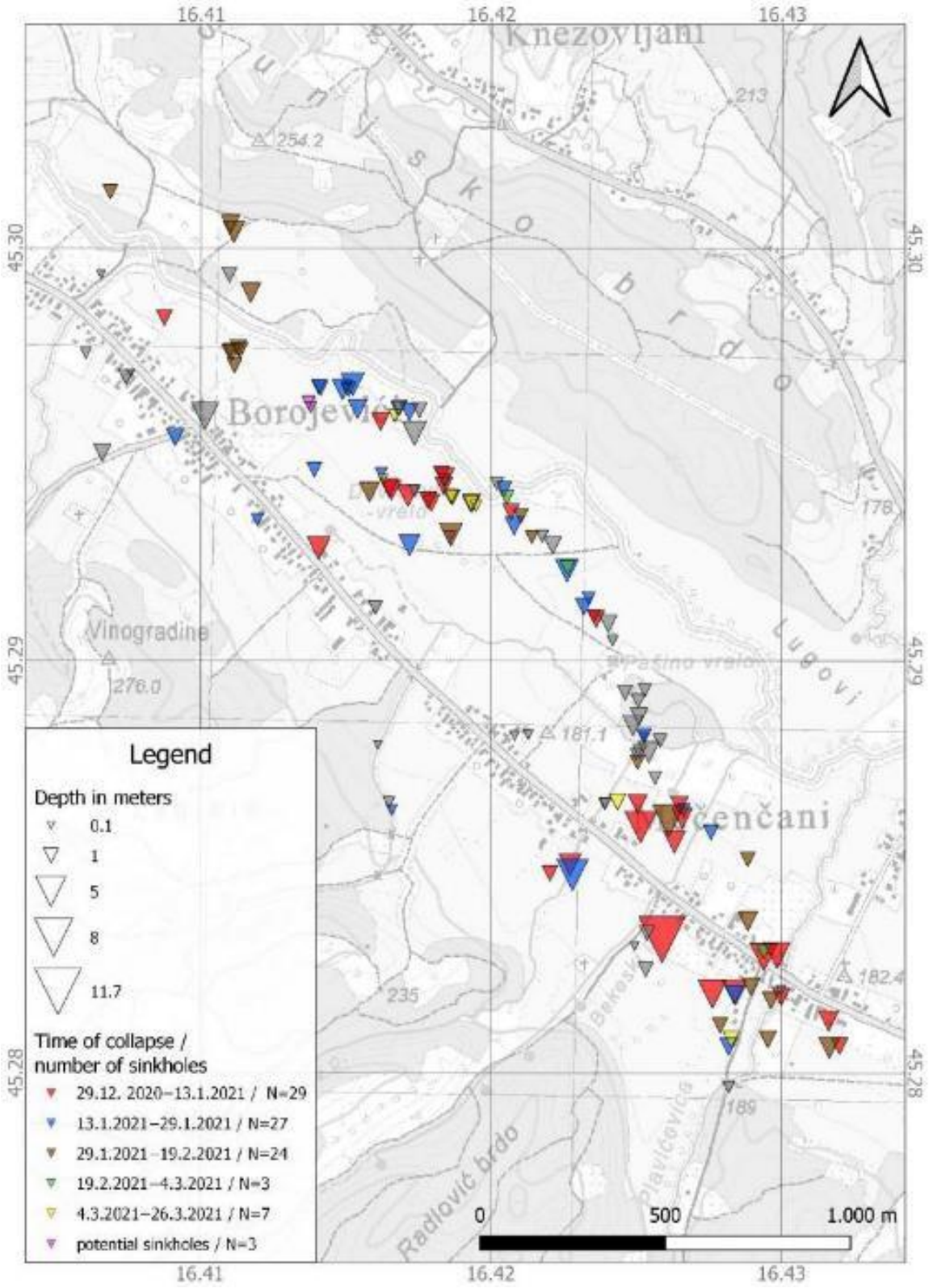

Figure 6.6 Spatio-temporal map of sinkholes in Borojevići and Mečenčani area and their depths on the topographic map.

Figure 6.7 Areal image of cover-collapse sinkholes in Mečenčani village (white – new sinkholes opened after M6.4 earthquake, black – fossil sinkholes opened before the Petrinja earthquake sequence). Image by Croatian Geological Survey.

Figure 6.8 Areal image of sinkholes north of Mečenčani village (white – new sinkholes opened after M6.4 earthquake, black – fossil sinkholes opened before the Petrinja earthquake sequence). Image by Croatian Geological Survey.

Figure 6.9 Areal image of sinkholes between Borojevići and Mečenčani villages (white – new sinkholes opened after M6.4 earthquake, black – fossil sinkholes opened before the Petrinja earthquake sequence). Image by Croatian Geological Survey.

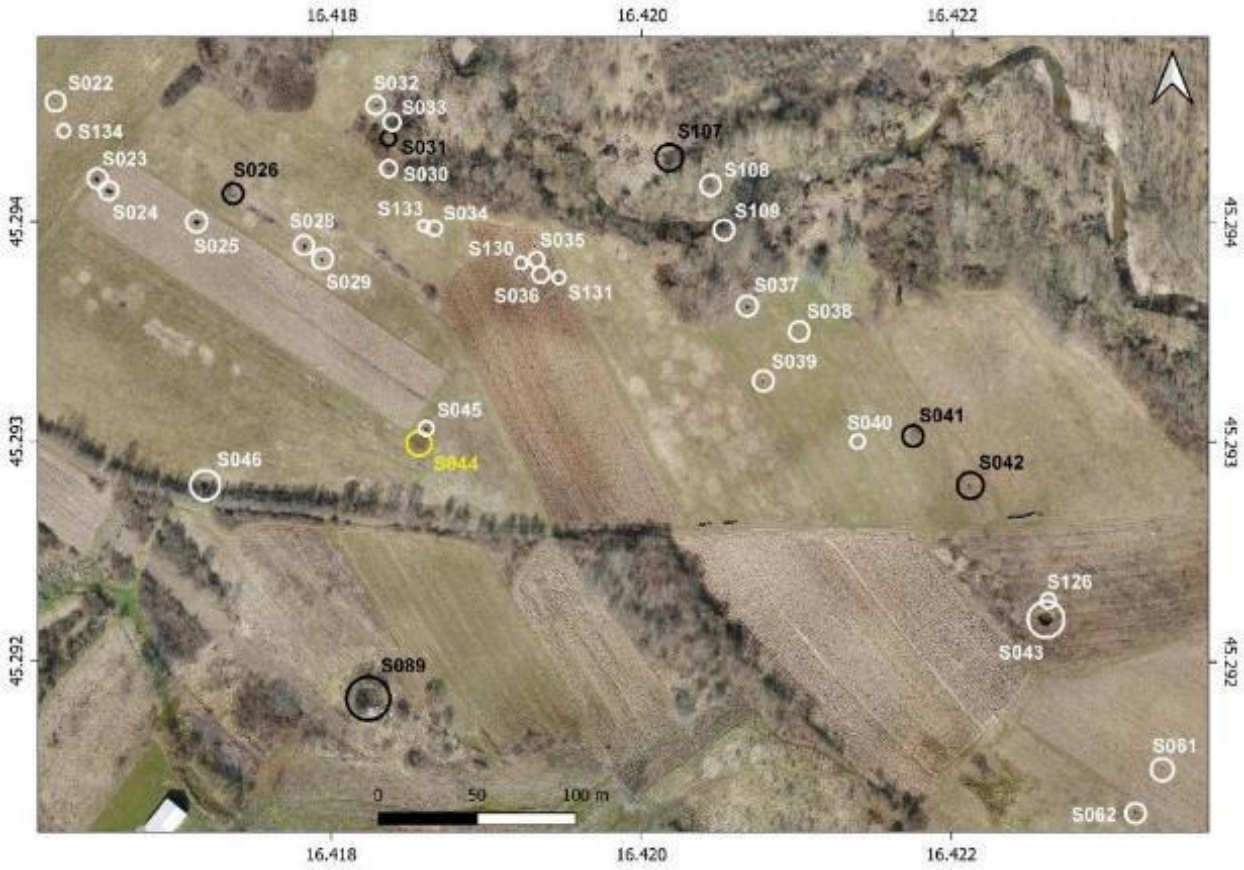

Figure 6.10 Areal image of sinkholes north of Borojevići village (white – new sinkholes opened after M6.4 earthquake, black – fossil sinkholes opened before the Petrinja earthquake sequence, yellow – potential locations of new cover-collapse sinkholes). Image by Croatian Geological Survey.

Figure 6.11 Areal image of sinkholes north of Borojevići village (white – new sinkholes opened after M6.4 earthquake, black – fossil sinkholes opened before the Petrinja earthquake sequence, yellow – potential locations of new cover-collapse sinkholes). Image by Croatian Geological Survey.

6.3 Hydrogeological characteristics of the Mečenčani and Borojevići area

The Sunja river valley in Mečenčani and Borojevići represents a flat area covered with Quaternary deposits of sand, silt, and clay on average 10 m thick. The material has low permeability but contains a certain amount of water and forms an unconfined aquifer from which it is possible to exploit a smaller amount of water. For this reason, most households use water from shallow dug wells with an average depth of about 8 meters (**Figure 6.12**). The fluctuation of groundwater level in the alluvial aquifer during dry and wet periods is about 2 m. The alluvial aquifer is underlain by a well-permeable confined karst aquifer in which the water pressure during wet periods becomes

subartesian to artesian. The groundwater level fluctuation in the karst aquifer is slightly less than in the alluvial aquifer, except near the Pašino vrelo pumping station, where both aquifers are strongly influenced by the well operation regime, i.e., the amount of pumping rate, which is 38 l/s on average.

These two aquifers are hydraulically connected, and pressure changes in one aquifer cause changes in hydraulic conditions in the other. They form a single aquifer system (**Figure 6.13**). The recharge of the karst aquifer is almost exclusively done through precipitation falling on the nearby hills where the Badenian Lithothamnium limestones and calcarenites crop out. Discharge of the karst aquifer takes place in the spring of Pašino vrelo. Next to the spring couple of deep wells were made, from which water is pumped for the public water supply. The spring of Pašino vrelo is a fossil cover-collapse sinkhole, which at its bottom has a direct connection with the karstified carbonate aquifer. Close to the Pašino vrelo spring, several other springs with a similar origin also play the role of discharge points.

The earthquake of December 29, 2020, occurred during a period of high waters. The water level in the alluvial aquifer was very close to the surface, and in the karst aquifer, artesian conditions prevailed. The piezometric level was about ten centimeters above the surface (**Table 6.1**).

Figure 6.12 a) Typical shallow well in an alluvial aquifer (depth 8 m, shallow well 3 in **Table 6.1**; 45.28154N, 16.43189E), b) Piezometer in a karst aquifer (depth 150 m; 45.29028N, 16.41797E).

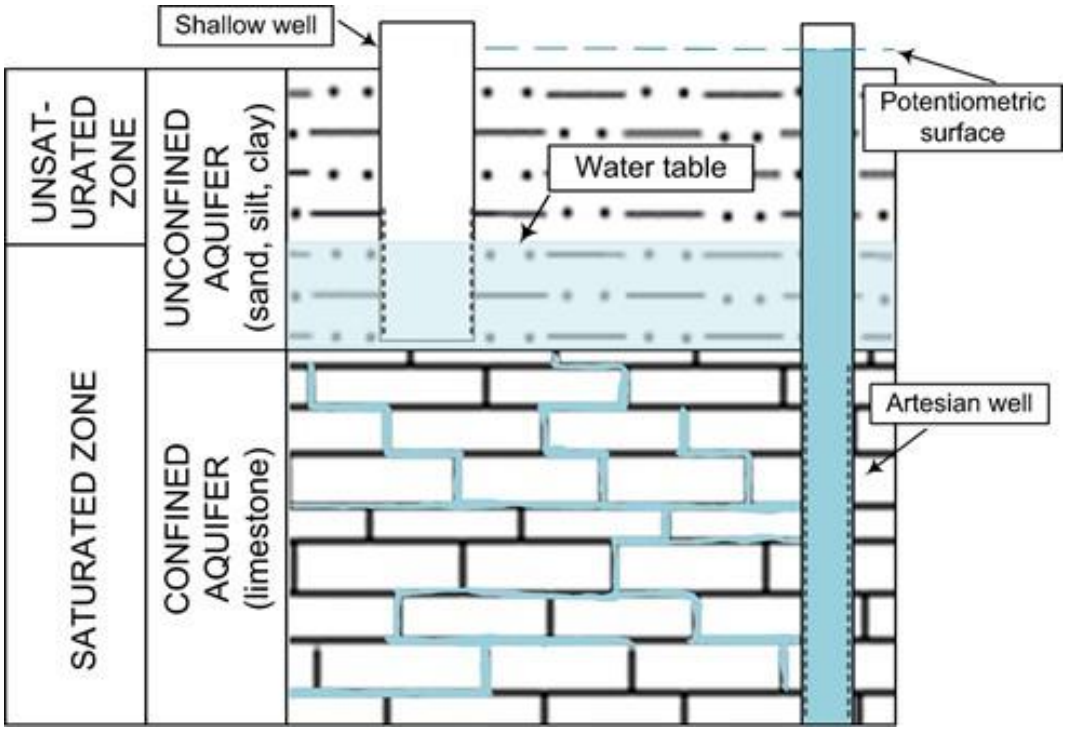

Figure 6.13 A conceptual model of hydrological condition in aquifer system during the earthquake (Mečenčani, Croatia).

Table 6.1 Position of three piezometers and three shallow wells located within the study area with their depths, terrain elevation, and groundwater level measured on February 9, 2021. All piezometers, including the shallowest one, penetrated the confined carbonate aquifer. Still, artesian pressure was recorded only in Piezometer 3 since the other two are close to the operating pumping site.

SITE	Latitude N	Longitude E	Depth (m)	Terrain elev. (m a.s.l.)	Water level February 9, 2021 (m a.s.l.)
Piezometer 1	45.29028	16.41797	150.0	183.5	183.59
Piezometer 2	45.28965	16.42395	28.0	178.6	175.65
Piezometer 3	45.28980	16.42342	10.0	178.9	176.08
Shallow well 1	45.29558	16.41006	14.0	191.4	185.98
Shallow well 2	45.28868	16.41876	10.0	185.5	184.63
Shallow well 3	45.28154	16.43189	8.0	183.4	179.95

6.4 Geotechnical and Geophysical Investigation Works

GEER team performed geotechnical and geophysical investigations in the zone impacted by numerous sinkhole collapses. Chapter 10 describes details of the extent of complementary investigation works. Local companies performed compound electrical resistivity tomography (ERT), Multichannel Analysis of Surface Waves (MASW), and borehole drilling. At the same time, the geotechnical laboratory at the University of Zagreb, Faculty of Mining, Geology and Petroleum Engineering conducted laboratory index testing of soil samples, and GEER team members analyzed data during March 2021. Two nanometric sensors for measuring horizontal to vertical spectral ratio were brought to the site by the GEER team from Natural Hazards Engineering Research Infrastructure (NHERI) RAPID facility at the University of Washington, Seattle, USA. An overview of complementary investigation works is shown in **Figure 6.14** on a geological map of the area. The GEER team performed 51 nanometric readings of ambient noise, five geotechnical boreholes, two MASW profiles, and one compound electrical resistivity tomography (ERT) profile. **Figure 6.14** shows the global positioning of nanometric and boreholes, while a detailed description of soil properties on specific sites is in Chapter 10.

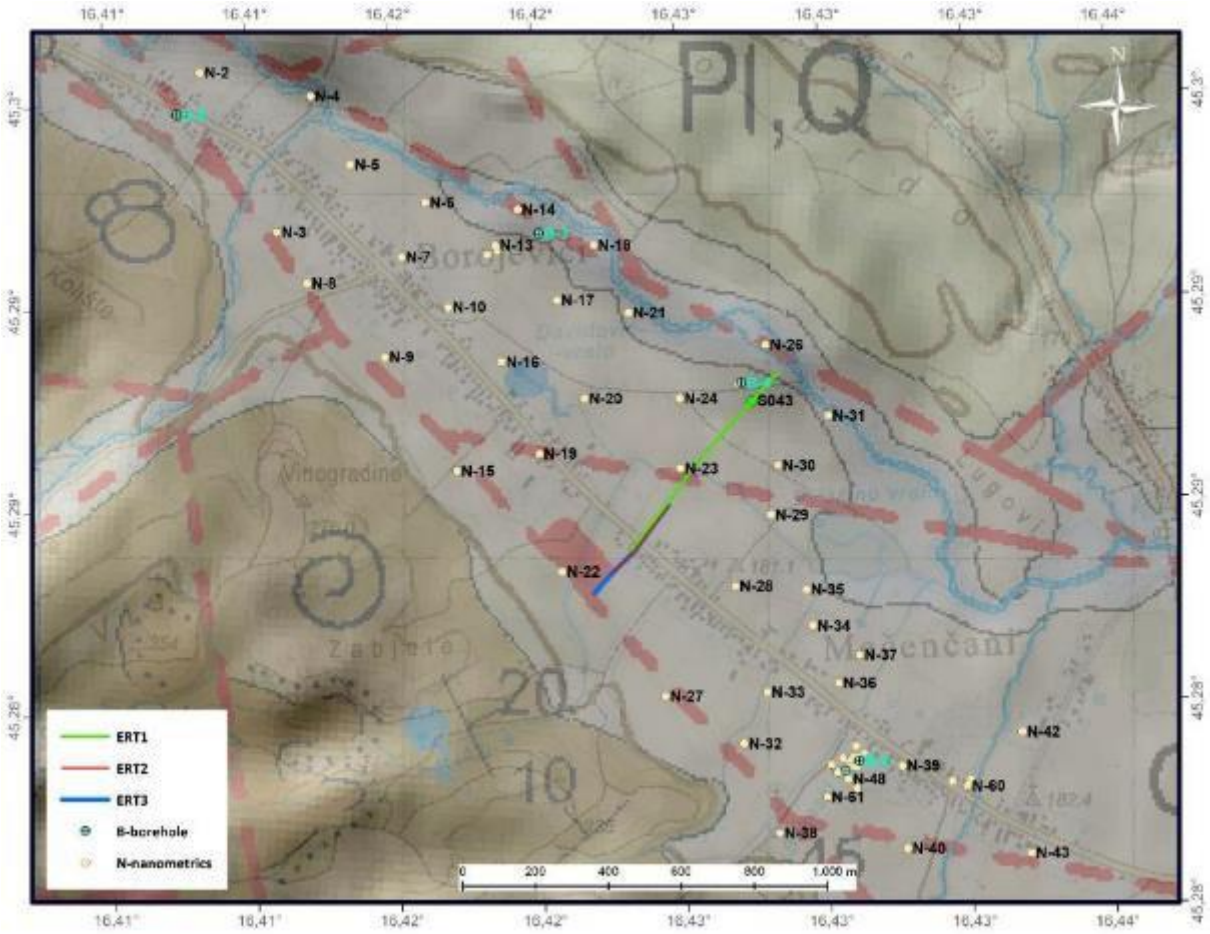

Figure 6.14 Overview of complementary investigation works on the geologic map (Basic geological map of the Republic of Croatia, Bosanski Novi sheet 1:100,000 – Šikić 2014).

Three electrical resistivity tomography (ERT) profiles were recorded by GEER team members from the Croatian Geological Survey (**Figures 6.14** and **6.15**). The POLARES 2.0 system with Wenner–Schlumberger array recorded all profiles, while interpretation and 2D visualization utilized Res2Dinvx64 software. ERT-1 profile was oriented 43–223°, 630 m long with 10 m distance between electrodes, and crosses perpendicularly from the Sunja river through the area between Mečenčani and Borojevići towards the hill at SW. The electrical resistivity profile detected a couple of predominately fossil sinkholes. To obtain a better resolution, two additional profiles with the same orientation, ERT-2 and ERT-3, were recorded with a distance of 5 m between the electrodes and lengths of 235 and 315 m.

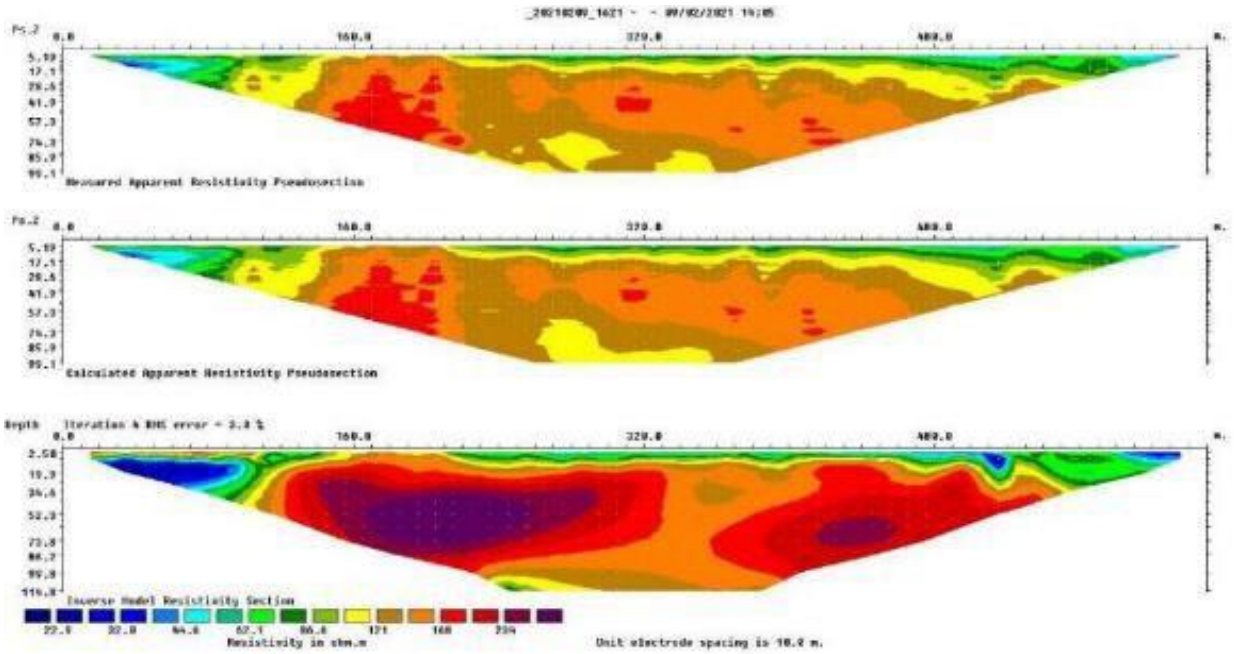

Figure 6.15 Electrical resistivity tomography (ERT) profiles recorded in the area between Mečenčani and Borojevići (left side of profiles NE, right side SW). For the position of profiles, see Figure 11.

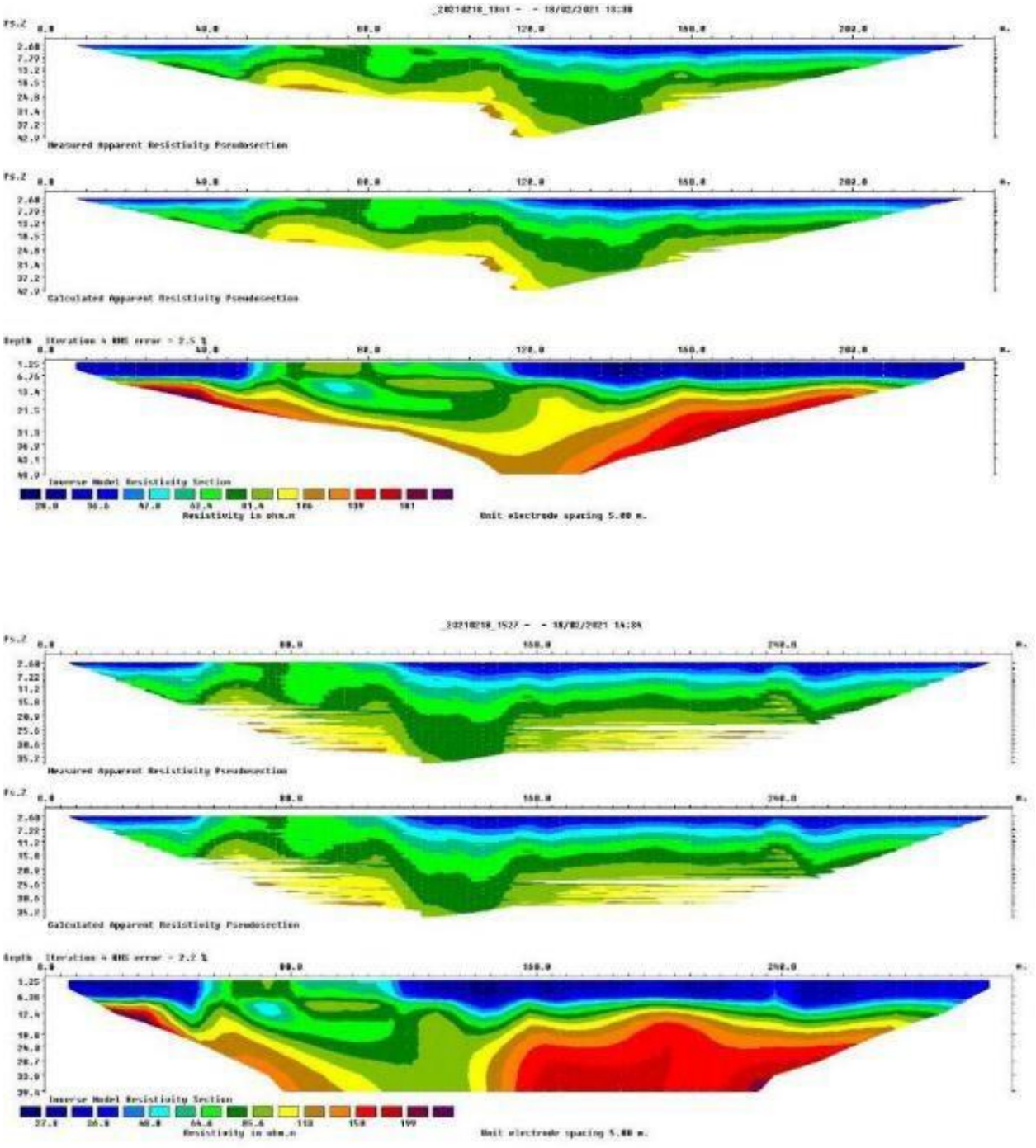

Figure 6.15 (cont.) Electrical resistivity tomography (ERT) profiles recorded in the area between Mečenčani and Borojevići (left side of profiles NE, right side SW). For the position of profiles, see Figure 11.

An HVSR analysis is shown in **Figure 6.16** that sorts approximate depths of karstic bedrock with colors. Although the research performed at this stage is a unique process described in Chapter 10, it should be noted that the fundamental resonant frequency f_0 determination was challenging

for some positions. Therefore, the analysis accuracy may be low. However, a few reliable results yielded representative data of the cover layer's relatively low thicknesses, which we detected for positions in proximity and along the Sunja river. We detected karst at deeper levels in the area between Mečenčani and Borojevići, and thicker cover in these locations could explain the absence of new sinkholes. Geotechnical boreholes near Sunja river were performed until shallow depths because the manual drilling equipment had difficulties penetrating through the alluvial deposits of clayey gravel with up to 15 cm grain sizes. The actual depth of the karst was not detected, unlike the B-1 in Borojevići, where the karst depth correlates with the N-1 nanometric result.

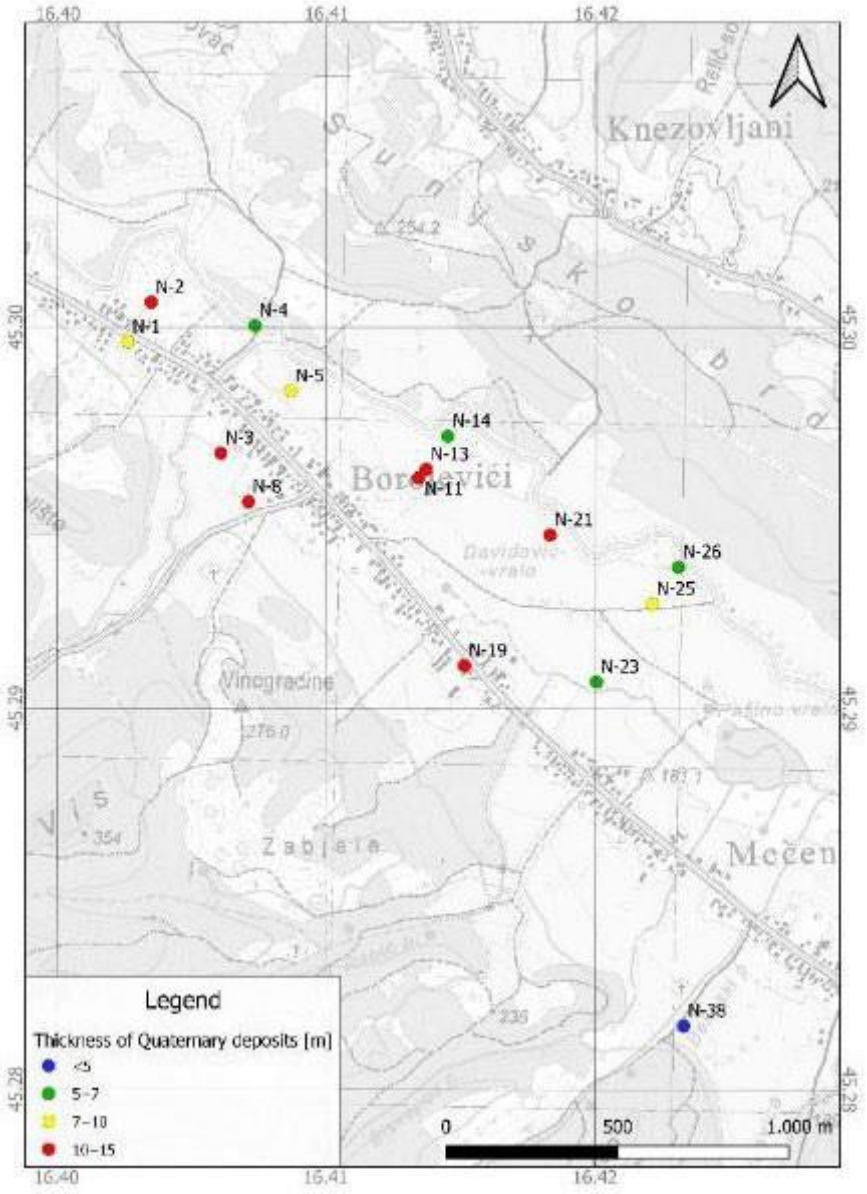

Figure 6.16 Estimated karst depths from HVSR measurement and analysis on a topographic map.

6.5. Detailed Description of Characteristic Sinkholes

This section shows lidar imagery, analysis, and conclusions from geotechnical and geophysical investigation works. The overview presents selected sinkholes, such as the largest sinkhole S001, sinkholes that collapsed in the vicinity of buildings and agricultural facilities, and smaller grouped sinkholes in Borojevići and near the Sunja river as well as fossil sinkholes. A comprehensive database of lidar images of around 60 sinkholes is available as open-source in DesignSafe Data Depot.

General Characterization of Sinkhole S001

The largest sinkhole, S001 (**Figure 6.17**) collapsed in Mečenčani between the January 4, 2021 afternoon and 13:00 h of January 5, more than 30 hours before the main aftershock, which took place at 18:01 on January 6 (M 4.9). the first subtle subsidence of the area was noticed by land-owners on January 4 afternoon. Two major foreshocks on December 28 (M 5.2 and M 4.7) and the main earthquake of December 29, 2020 (M 6.4) preceded a week before the S001 collapse. The surface soil collapsed at once into S001, forming a sinkhole about 15 m in diameter, followed by minor adjustments and collapses of walls, which remained sub-vertical. **Figure 6.18** shows snapshots from the video recorded on January 6, where the walls are collapsing with an unstable, brittle clay block of approximately 2–3 m, and S001 is widening (Vidić, 2021. Available at: https://www.youtube.com/watch?v=br-ocSaXlDgwww).

Figure 6.17 A giant sinkhole (S001) in the Mečenčani. The photograph was taken on March 15, 2021, during lidar imaging (45.283243N, 16.425887E).

GEER team did lidar imaging on March 15 and March 23. The GEER team recorded an MASW profile in the vicinity of S001, two boreholes B-1 and B-2, eight nanometric sensors (N-51 to N-58) were measuring ambient noise for approximately 25–30 minutes positioned closely around S001 and seven nanometric in the vicinity (N-44 to N-49). **Figure 6.19** shows a schematic of data collection and positions of geotechnical and geophysical investigation works. The GEEER team was measuring water levels in geotechnical boreholes during drilling, 3 hours and three days after the drilling. Water depth was also measured in a well on the same compound approximately 5 m away from S001. The water level in S001 was measured on February 15, 2021, as 2.5 m below the ground surface, and it is relatively stable since its opening. The maximum depth of the sinkhole measured from the ground surface to the bottom of the deposited collapsed material using custom-built weight was 11.7 m.

a) The collapse of the edge of a larger unstable clay block.

b) Upper portions of the block are falling.

c) Large block collapse.

d) Material sinks under the water

Figure 6.18. S001 brittle wall collapse sequence on January 6, 2021 (45.2833444N, 16.4259639E) (Vidić, 2021. Available atČ https://www.youtube.com/watch?v=br-ocSaXlDgwww).

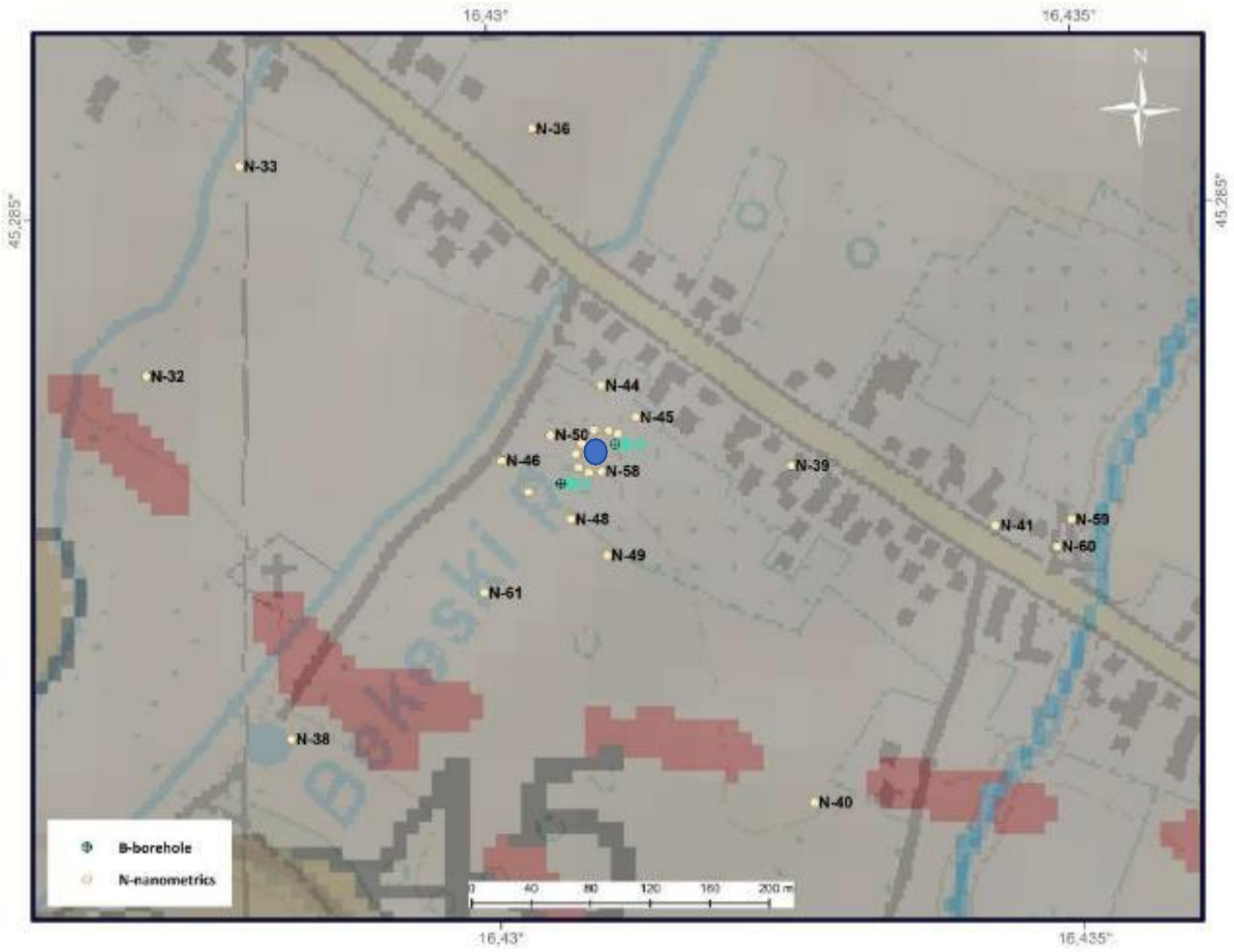

Figure 6.19 Positions of geotechnical and geophysical investigation works around S001 on the topographic map background.

Morphological and Spatial Characteristics of S001

S001 is characterized by vertical walls in brown clay, with sparse 30–60 cm thick lenses of round grain gravel. **Figure 6.20** shows a photograph taken by the lidar imaging positions and a sample scan. The bundle links 13 setups with 35 links with the bundled error 8 mm. **Figure 6.21** shows the top view where the longest axis diameter is about 24.55 m, and the largest diameter at the bottom of the scan is 21.865 m (**Figure 6.22**). The water depth is 2.507 m from the upper edge of the sinkhole, as shown in **Figure 6.23**. **Figure 6.24** shows an example of sinkhole volume calculation from terrestrial lidar point cloud data. However, due to the relatively high water level, the GEER team could not obtain information about the sinkhole contours under the water.

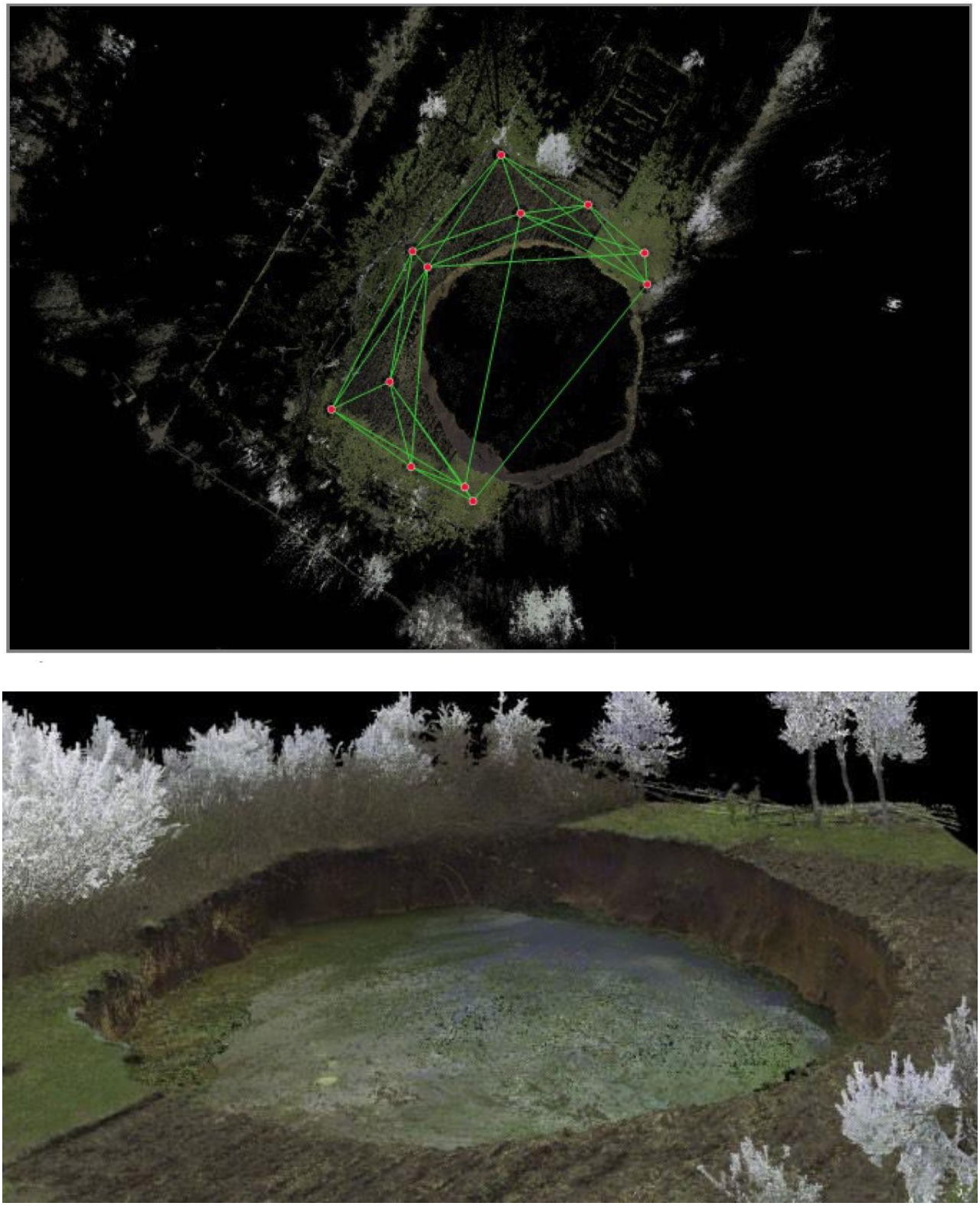

Figure 6.20 Lidar bundle with 13 setups and 35 links around S001 (45.2833444N, 16.4259639E).

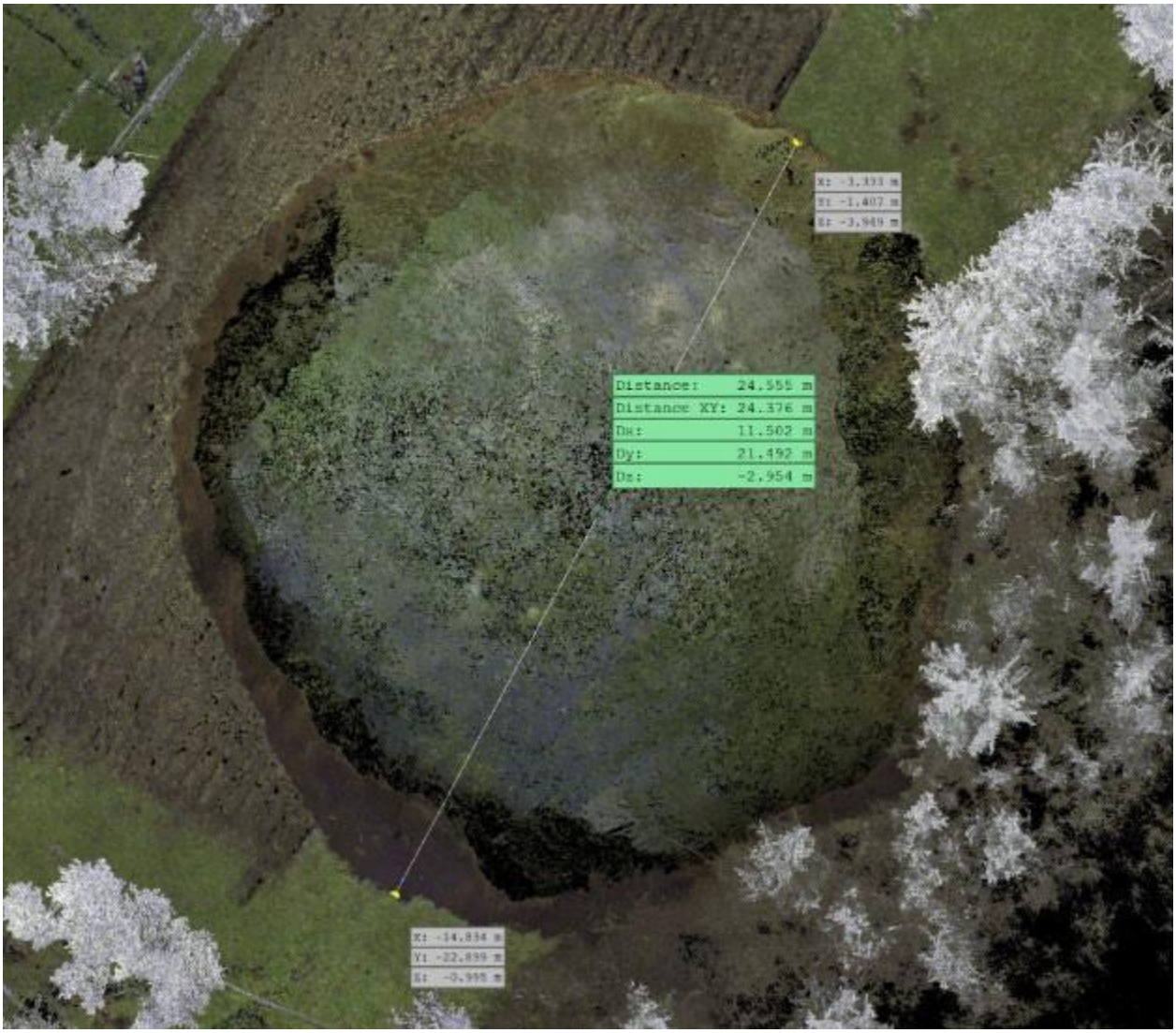

Figure 6.21 Top view diameter of S001 from lidar scan (45.2833444N, 16.4259639E).

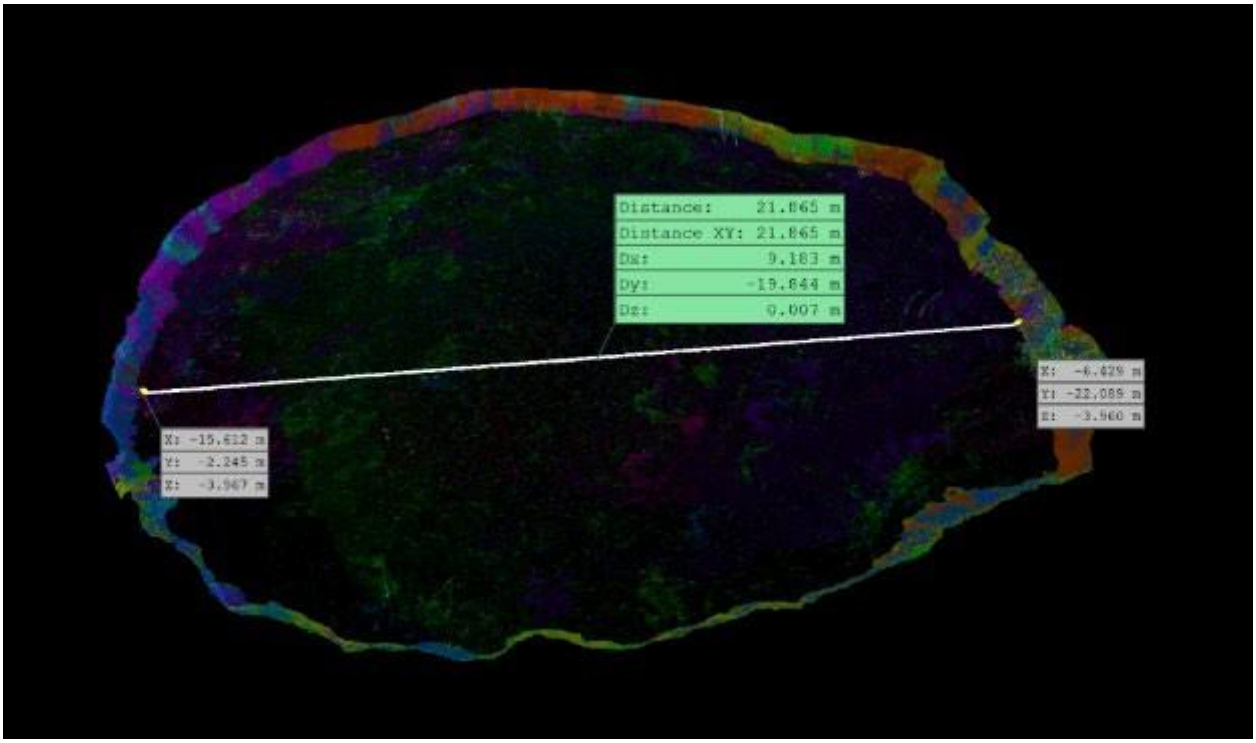

Figure 6.22 Diameter at the lidar scan on the bottom level of S001 (45.2833444N, 16.4259639E).

(a)

(b)

Figure 6.23 Y-axis cross-section scans with dimensions of S001 (45.2833444N, 16.4259639E).

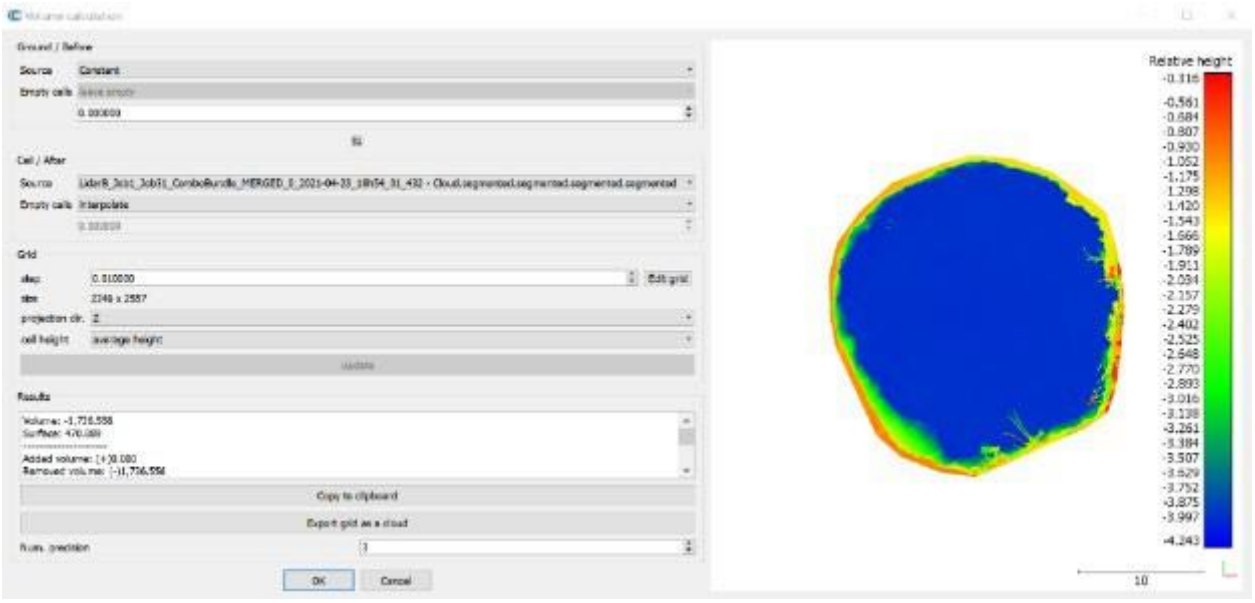

Figure 6.24 Volume calculations of S001 (45.2833444N, 16.4259639E).

Geotechnical and Geophysical Investigation Results of Soil around S001

Insight into two geotechnical boreholes reveals that soil consists of 0.5 of fill, 3.5 of sandy lean, and fat clay that is firm to stiff, containing sparse traces of limestone particles up to 20 mm in diameter, with sharp edges (**Figure 6.25)**. Limestone particles are distinct and white. Below is stiff to very stiff clay, interlayered by very moist clay with gravel. Boreholes were drilled without heavy machinery and stopped where the equipment could not penetrate stiffer layers at approximately 8,0 m depth. Lower layers are in B-1 gray lean marly clay, with low plasticity and high stiffness. Bedrock or cobbles appeared below 8 m, where also the Standard Penetration Test equipment bounced off without penetration.

Multichannel Analysis of Surface Waves (MASW) has been performed just along the edge of S001. **Figure 6.26** shows a two-dimensional interpretation of the MASW profile near S001, where lower shear wave velocities of 180–220 m/s occur until 5–6 m depth, under which are slightly higher velocities 300–400 m/s between 6 and 10 m. Relatively uniform strata down to 25 m are shown in green and yellow colors, which has heterogeneous 400–500 m/s velocities. It can be concluded that the compact rock layer appears below 25 m, which is geologically characterized as karst. Comparing to MASW profiles, indeed, shear wave velocities increase at that depth. Detailed presentation of investigation works is in Chapter 10.

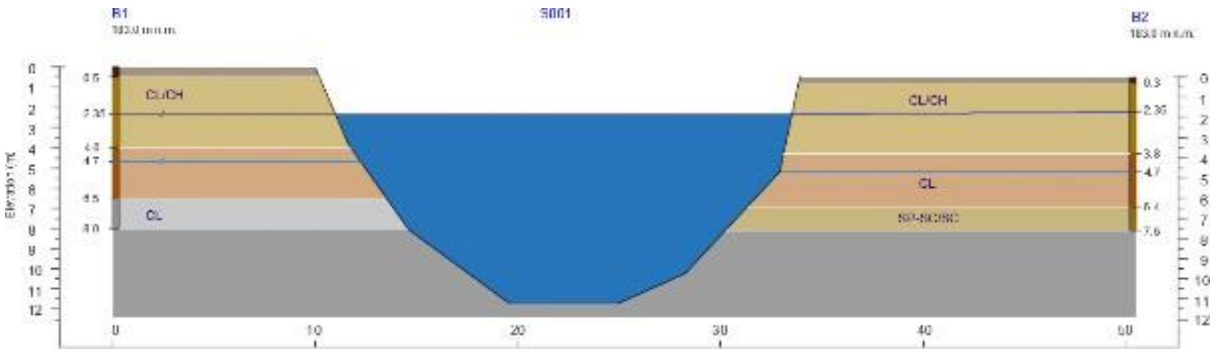

Figure 6.25 Soil profile around S001, dimensions are given in mm (45.2833444N, 16.4259639E).

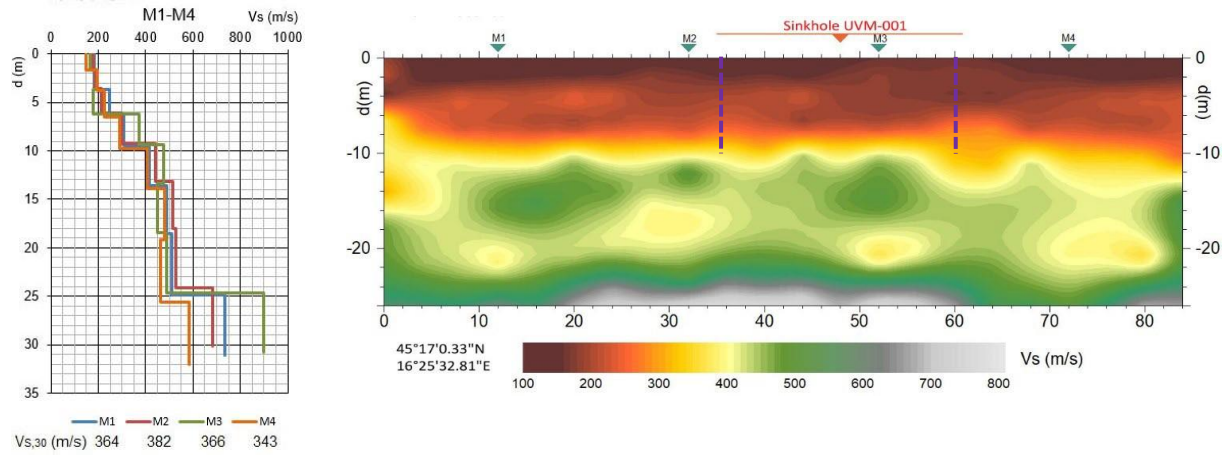

Figure 6.26 MASW profile with a sketch of S001 to the depth of 11.2 m (45.2833444N, 16.4259639E).

Horizontal-to-Vertical Spectral Ratio (HVSR) analysis obtained curves which are not showing a distinct peak to get f_0 frequency. A potential rock stratum was approximately determined using the shear wave velocity obtained from MASW and expression using the quarter-wavelength equation:

$$H=v_{s,avg}/(4\cdot f_0)$$

where H is the thickness of the sediment above the bedrock, $v_{s,avg}$ is the average shear wave velocity over the sediment, and f_0 is the fundamental resonant frequency. **Table 6.2** gives an overview of estimated depths, and **Table 6.3** shows HVSR analysis results for each. The analysis indicates HVSR uncertainties when handling weathered karst mixed with stiff clays and clay mixed with larger granite gravel cobbles that were found in boreholes as lenses within clays at different heights. Granite cobbles were detected in the broader area as well, even sometimes on the ground surface. The density of weathered karst is 2290 kg/m^3 and 2062 kg/m^3, which indicates a significant presence of voids in intact rock. Despite the challenges presented here, HVRS shows two material horizons at 4–5 m north from S001 and 10–12 m depth south from S001, which

correlates with boreholes and MASW data. Additional seven nanometric measurements also indicate clay cover depths from 5.4 m to 9.8 m, where N-50 between S001 and S065 suggests the interface depth at *H*=5.4 m.

Table 6.2 Calculated depths of karstic formation around the sinkholes.

Nanometrics Name	Longitude	Latitude	f_0	$v_{s,avg}$ (m/s)	H (m)
N-50	45.2834833N	16.4255583E	12	220	4.6
N-51	45.2834861N	16.4261361E	12.4	220	4.4
N-52	45.2835056N	16.4260583E	12.1	220	4.5
N-53	45.2835111N	16.4259306E	5.64	220	9.8
N-54	45.2834333N	16.4258250E			
N-55	45.2833667N	16.4257750E	5.45	220	10.1
N-56	45.2832833N	16.4257944E	4.55	220	12.1
N-57	45.2832528N	16.4258806E	4.96	220	11.1
N-58	45.2832583N	16.4259917E	5	220	11.0

Table 6.3 HVRS analysis for nanometric surrounding S001.

N-51: f_0 = 12.4 (S001)	N-52: f_0 =12.1 (S001)
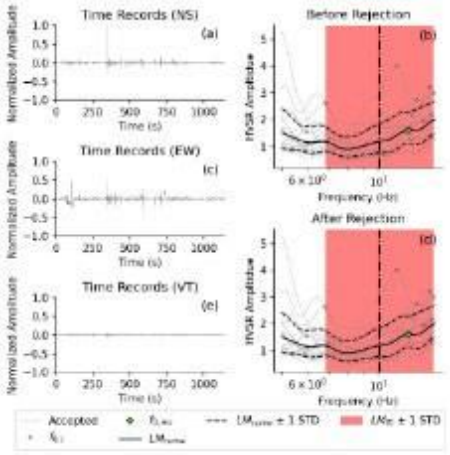	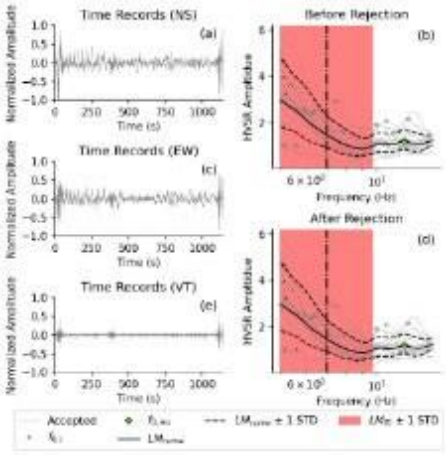

Table 6.3 (cont.) HVRS analysis for nanometric surrounding S001.

N-53: f_0 = 5.64 (S001) 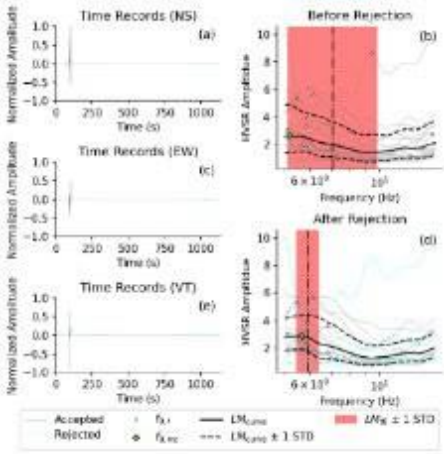	N-54: f_0 = no data except for 2.19 (S001)
N-55: f_0 = 5.45 (S001) 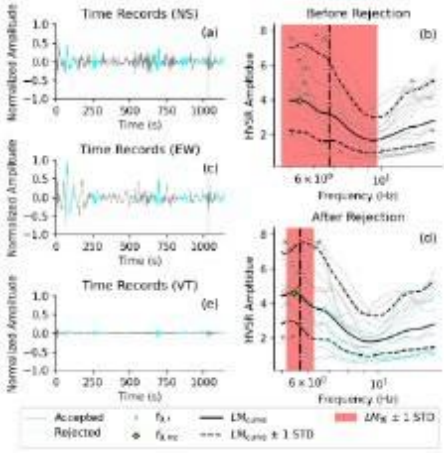	N-56: f_0 = 4.55 (S001) 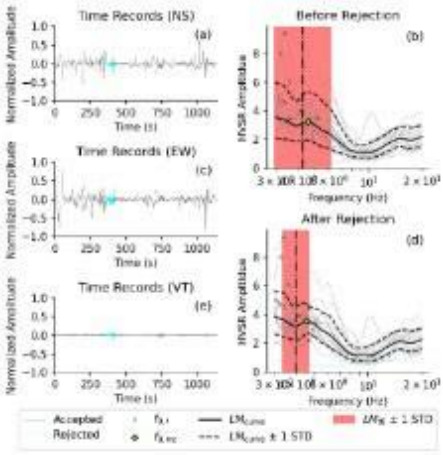
N-57: f_0 = 5.96 (S001) 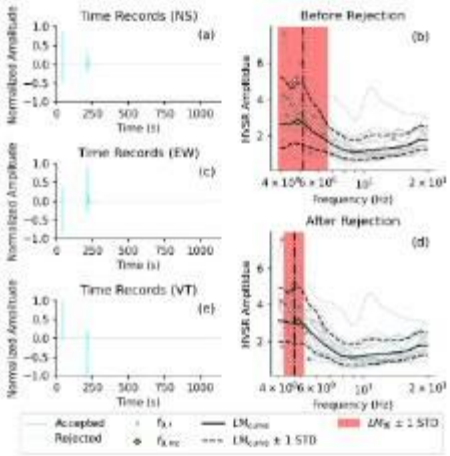	N-58: f_0 = 5.0 (S001) 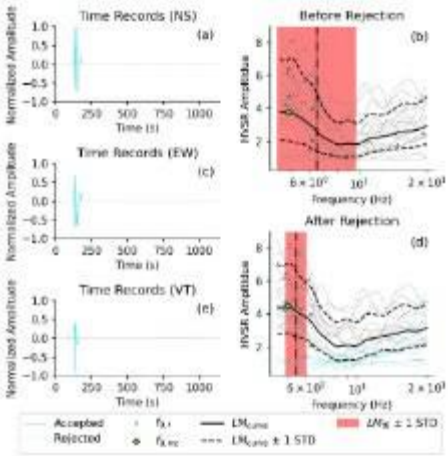

Groundwater Levels near S001

Detected groundwater levels in boreholes B-1 and B-2 are shown in **Table 6.4**. Groundwater rises from ~-5.0 to ~-2.2 m from the ground surface with different dynamics. Additionally, the well water levels placed ~5 m from S001 were consistent at ~-5.0 m. The groundwater level rise in boreholes may occur due to flow from adjacent saturated soil or artesian pressure in the subsurface karstic formation. Since piezometers are not installed at the site, the groundwater pressure is not measured now.

Table 6.4 Measured levels of groundwater at different times and locations near S001

Description	G.W.L. (m below ground level)	Date	Time
Private Well	-5	3/23/2021	NPV*
BH B-1	-4.7	3/23/2021	10:30:00 AM (PPV**)
BH B-1	-2.25	3/23/2021	15:30 PM (NPV*)
BH B-1	-1.8	3/26/2021	NPV*
BH B-2	-5.2	3/23/2021	PPV**
BH B-2	-2.4	3/26/2021	NPV*

*NPV is the groundwater level.
**PPV is the groundwater level first appearance.

We estimated the degree of saturation using phase relationships for samples in B-1 and B-2. The specific gravity measurements were unreliable and yielded too low values in the lab, so we assumed an average value of Gs=2.75 instead. Results indicate unsaturated zone in B-1 at 2.0–2.3 depth at S_r=0.82, and saturated zone at 4.0–4.3 at S_r =1.0, 6.0–6.3 at S_r =0.96. Results relate to the behavior of the groundwater in B-1, which was detected at 4.7 m depth and rose to 2.25 m inthree hours. In B-2, unsaturated zone was detected at 1.0–1.3 at S_r=0.56, 4.0–4.3 at S_r =0.6 and 5.0–5.3 at S_r =0.62. Groundwater depth was stable at 5.2 m depth during March 23 and did not rise as in B-1 after a few hours, despite the proximity of both boreholes. Three days later, the groundwater indeed rose to 2.4 m below the ground surface in B-2.

6.5.6 Examples of Sinkholes Near Buildings

The GEER reconnaissance team recorded a total of 6 sinkholes that collapsed very close to buildings and greenhouses, including S001. Sinkhole S015 is the second-largest sinkhole in the backyard in Mečenčani, and the family house was tagged as non-livable. Another sinkhole, S014 collapsed under an old brick house. Three sinkholes, S053, S054, and S055, were relatively smaller in diameter but caused distress to a family that has greenhouses. The following section shows each sinkhole and lidar data.

Sinkhole S015

S015 collapsed on December 29, 2020, with the first subsidence noticed six hours after the main shock, followed by the opening of two cover-collapse structures (each about 1.5 m in diameter

and cca. 1 m deep) within the next three hours and further collapse and formation of united sinkhole until the morning of December 30. **Figure 6.27** shows a lidar bundle scan near a house, where **Figures 6.28** and **6.29** show measurements from point cloud data.

Figure 6.27 The lidar scan of S015 (45.282859N, 16.429841E).

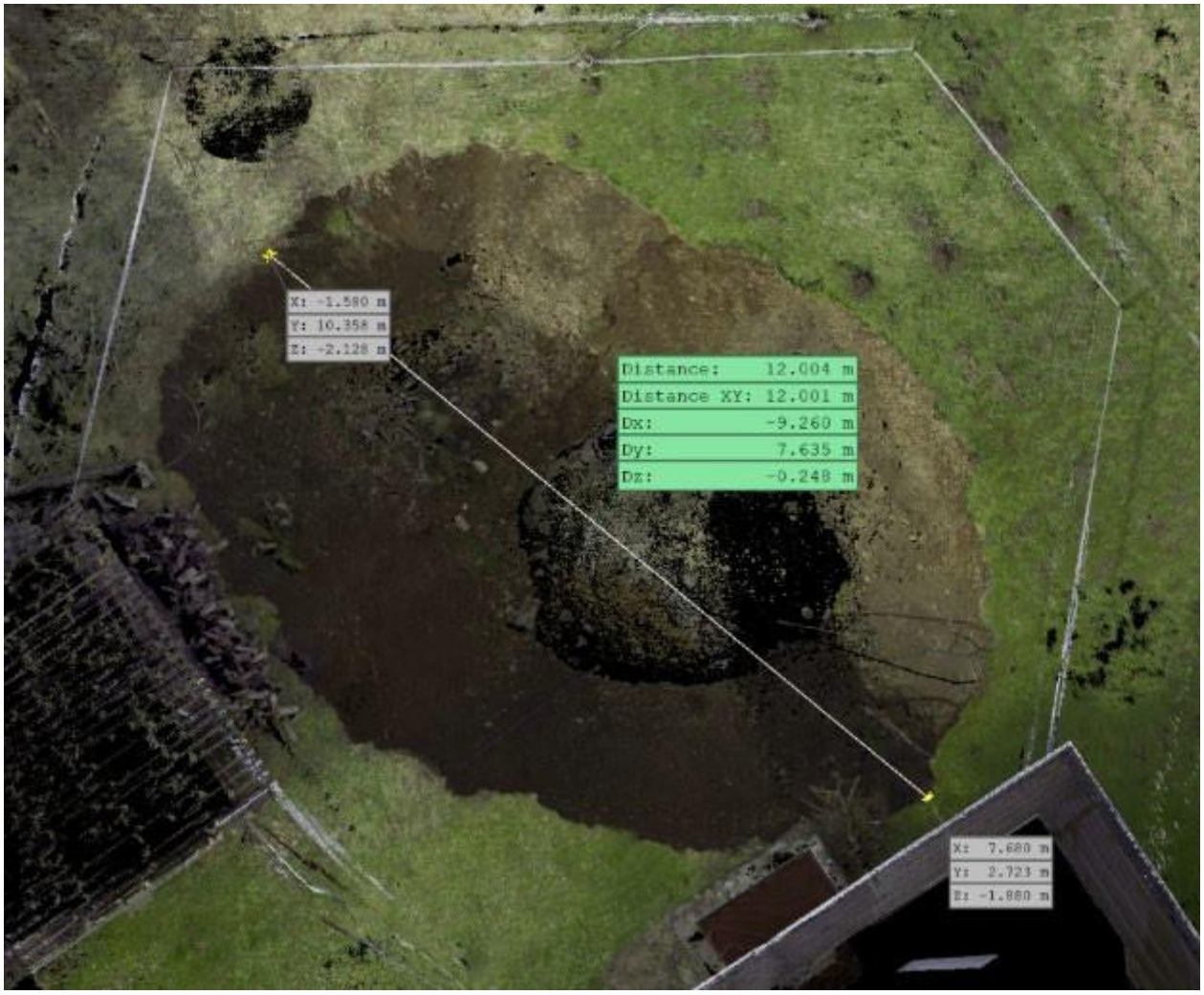

Figure 6.28 Top and bottom diameters from the lidar scan of S015 (45.282859N, 16.429841E).

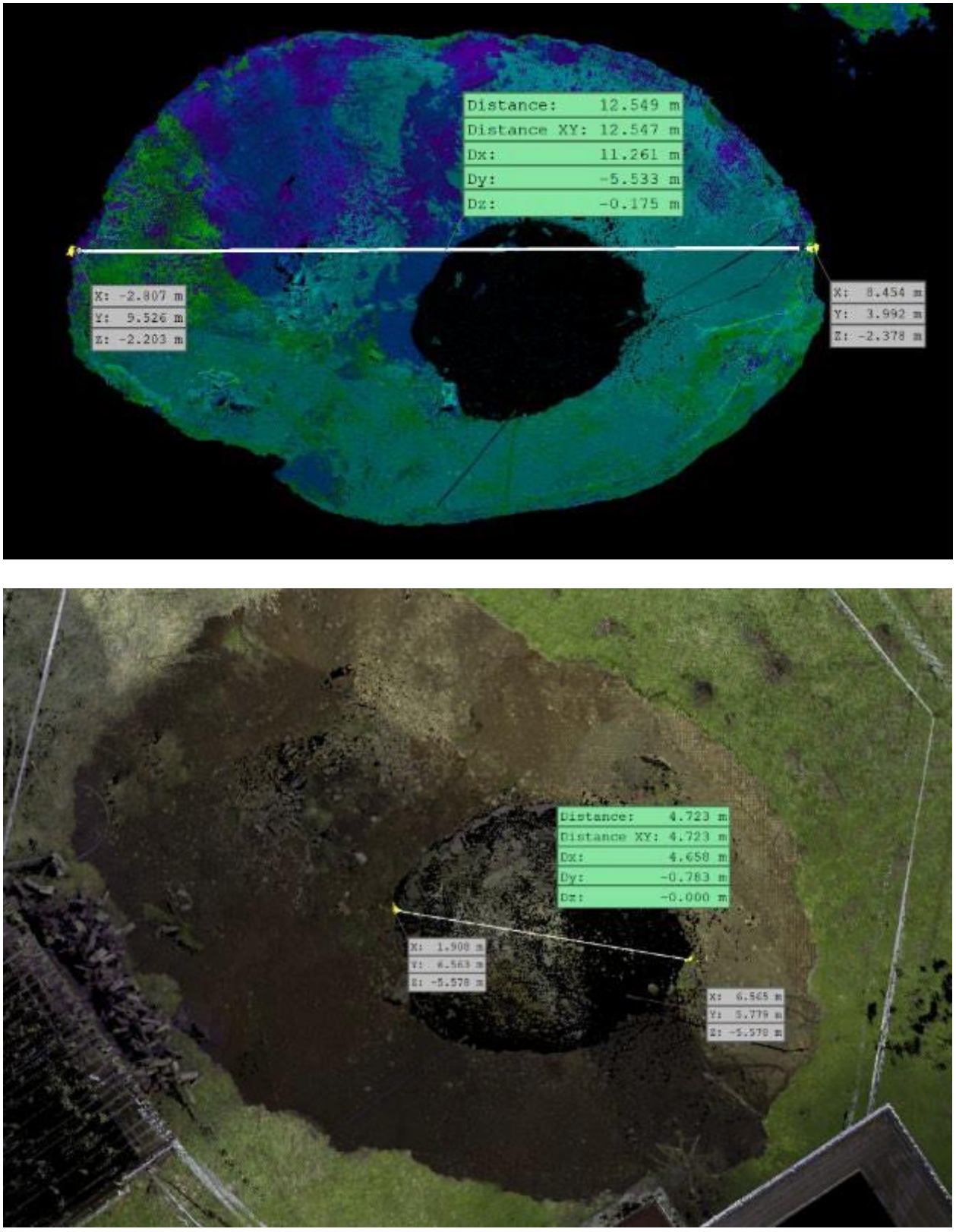

Figure 6.28 (cont.) Top and bottom diameters from the lidar scan of S015 (45.282859N, 16.429841E).

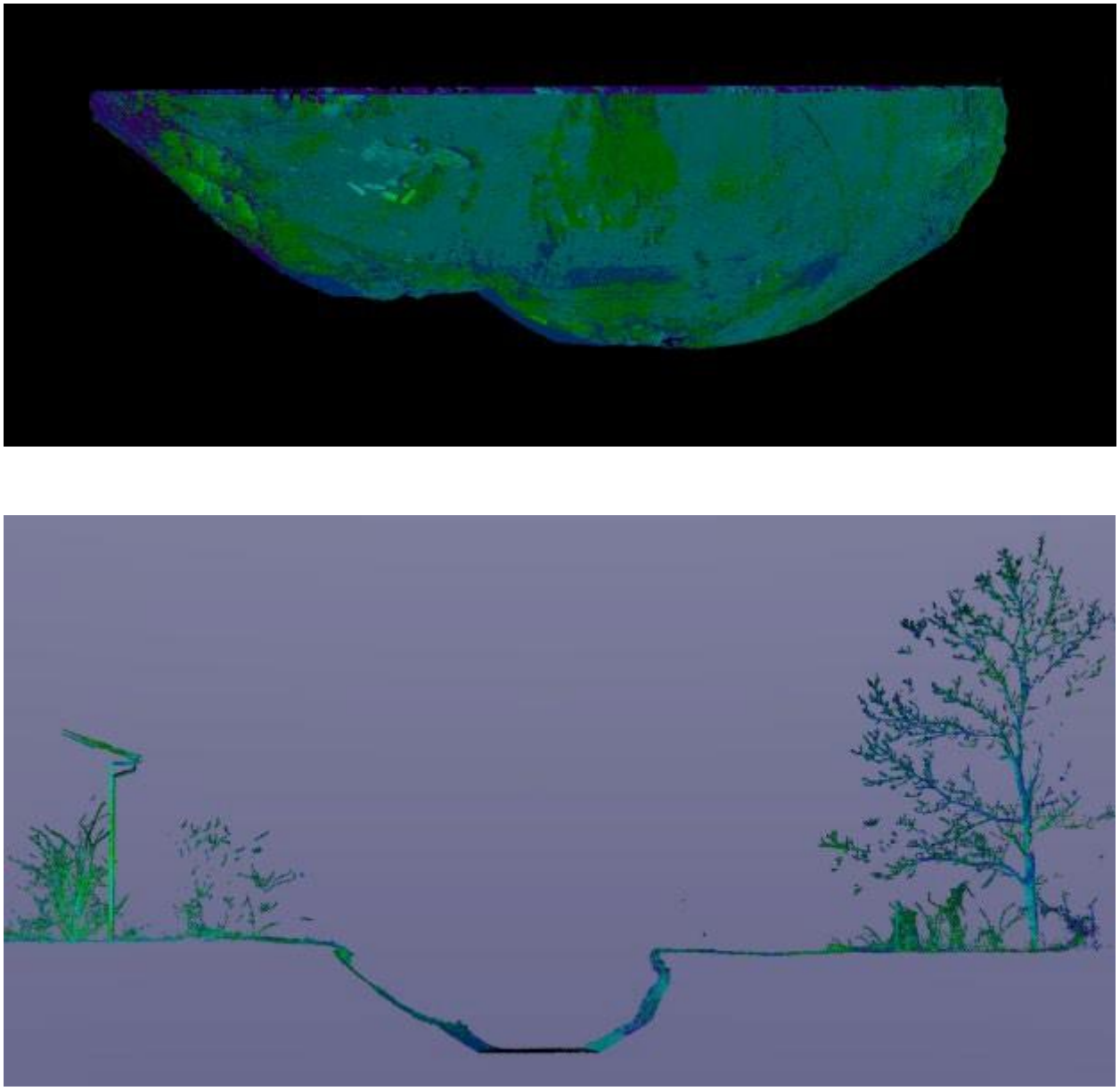

Figure 6.29 Below surface cross-sections from the lidar scan of S015 (45.282859N, 16.429841E).

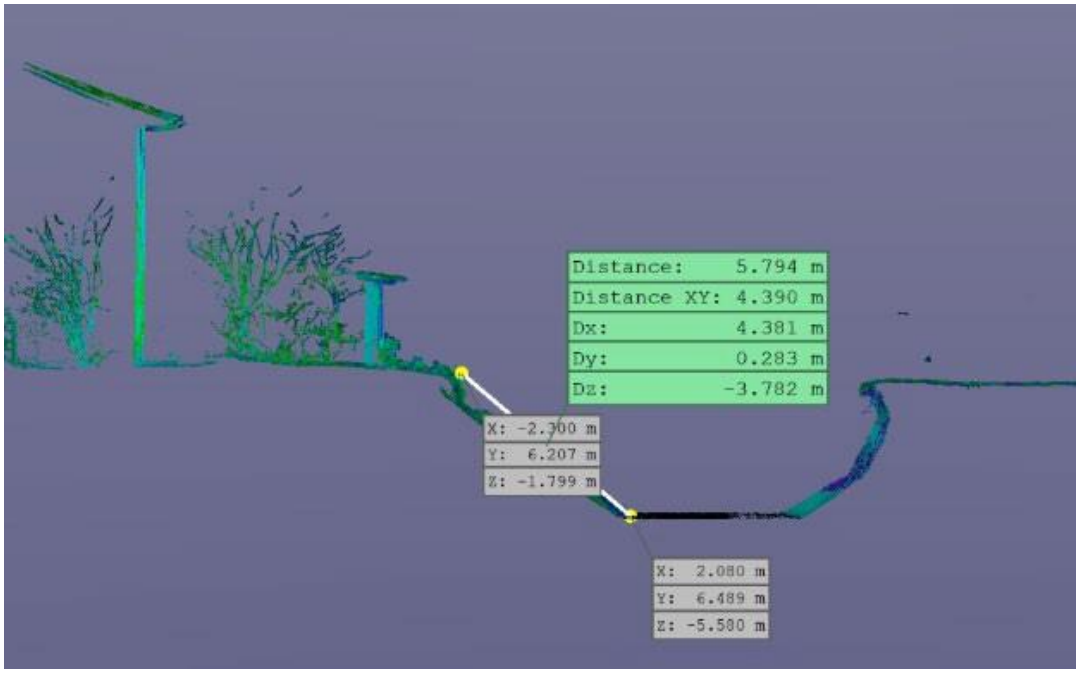

Figure 6.29 (cont.) Below surface cross-sections from the lidar scan of S015 (45.282859N, 16.429841E).

Sinkhole S014

Sinkhole S014 collapsed on December 31, 2020, near a brick wall family house, as shown in **Figures 6.30** and **6.31,** and is full of water. S014 caused floor slab and house walls failure, whose materials then fell into the sinkhole.

Figure 6.30 Street view of the house and S014 position (45.282822N, 16.429389E).

Figure 6.31 S014 images (45.282822N, 16.429389E).

Sinkholes S053, S054 and S055

Sinkholes S053, S054, and S055 have a relatively small diameter, as shown in **Figures 6.32** to **6.38**. Three sinkholes collapsed within an agricultural family compound in Mečenčani. S053 was just next to the family house wall, as shown in **Figure 6.32**. S054 and S055 collapsed near greenhouses.

Figure 6.32 S053 bundle image (45.281270N, 16.431618E).

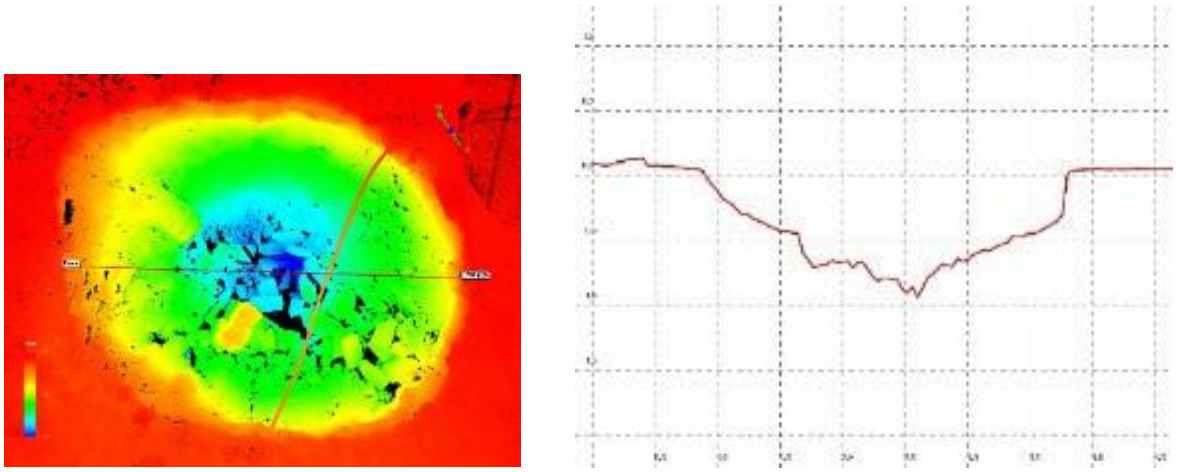

Figure 6.33 S053 Surface level measurement and cross-sectional profile (45.281270N, 16.431618E).

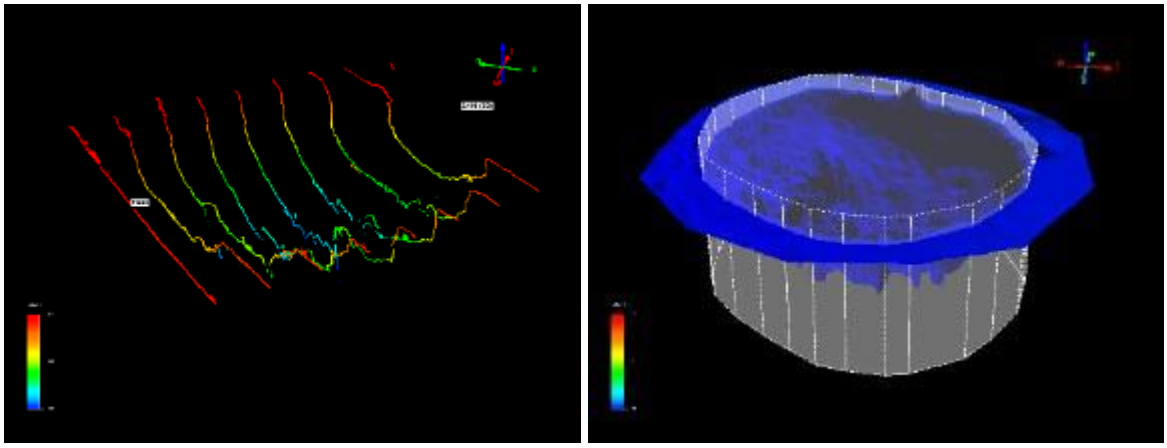

Figure 6.34 S053 Cross sections and volume estimate V=2.98 m^3 (45.281270N, 16.431618E).

Figure 6.35 S054 lidar scan bundle view (45.280665N, 16.431996E).

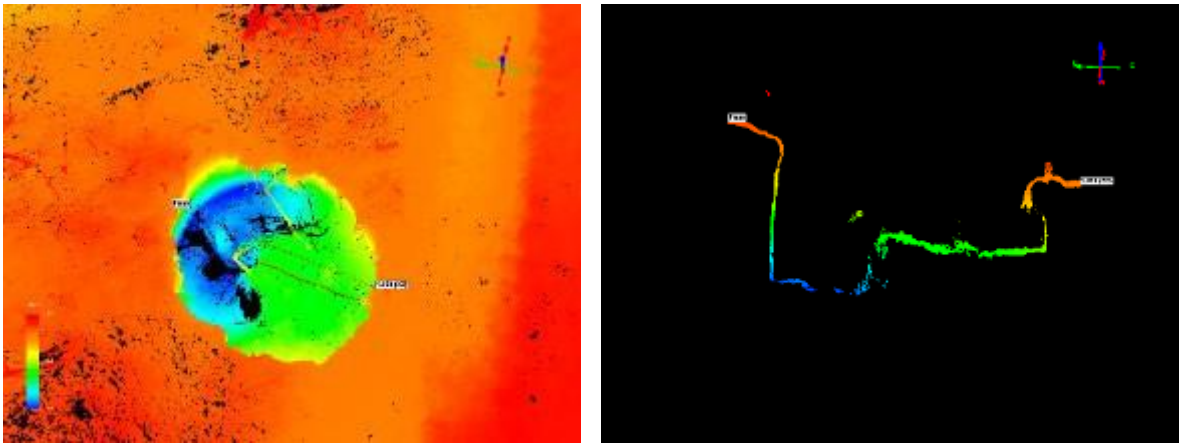

Figure 6.36 S054 plan view and cross section (45.280665N, 16.431996E).

Figure 6.37 S055 lidar scan bundle view (45.280618N, 16.431644E).

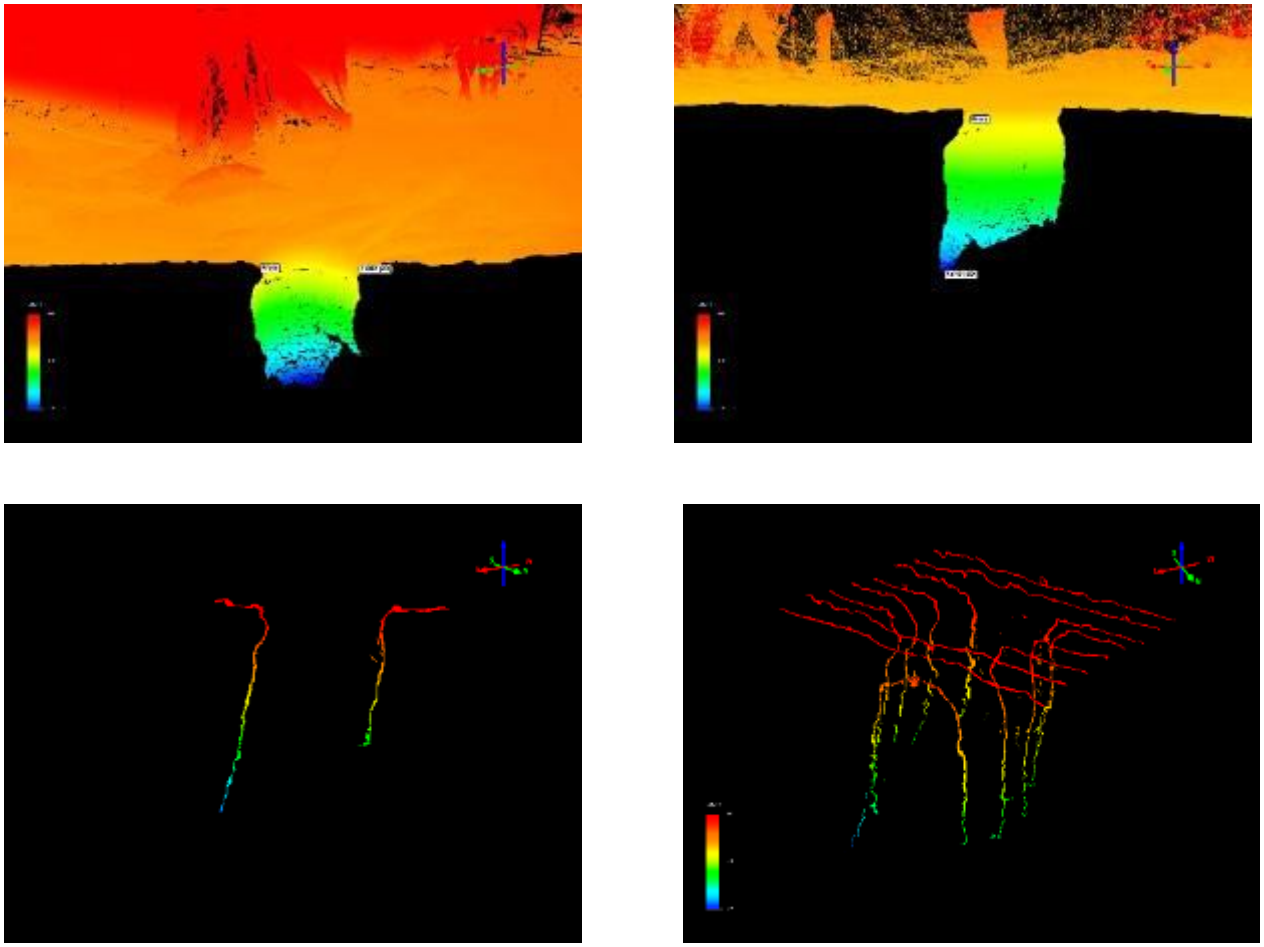

Figure 6.38 S055 cross sections (45.280618N, 16.431644E).

Sinkholes in Borojevići Area

Numerous sinkholes collapsed in Borojevići, where many are near and along the Sunja river. Sinkholes in this particular area are generally shallower and have a smaller diameter. **Figures 6.39** to **6.45** show a few typical examples of lidar scans and measurements. It was possible to bundle scans of two or three sinkholes into one in several locations, which provided a good idea about the qualitative spatial variability of sinkhole characteristics. Sinkholes were either similar or very different next to each other. In some locations, new sinkholes opened near fossil sinkholes. Such variability depicts the heterogeneity and unpredictability of underlying karstic formations in these locations.

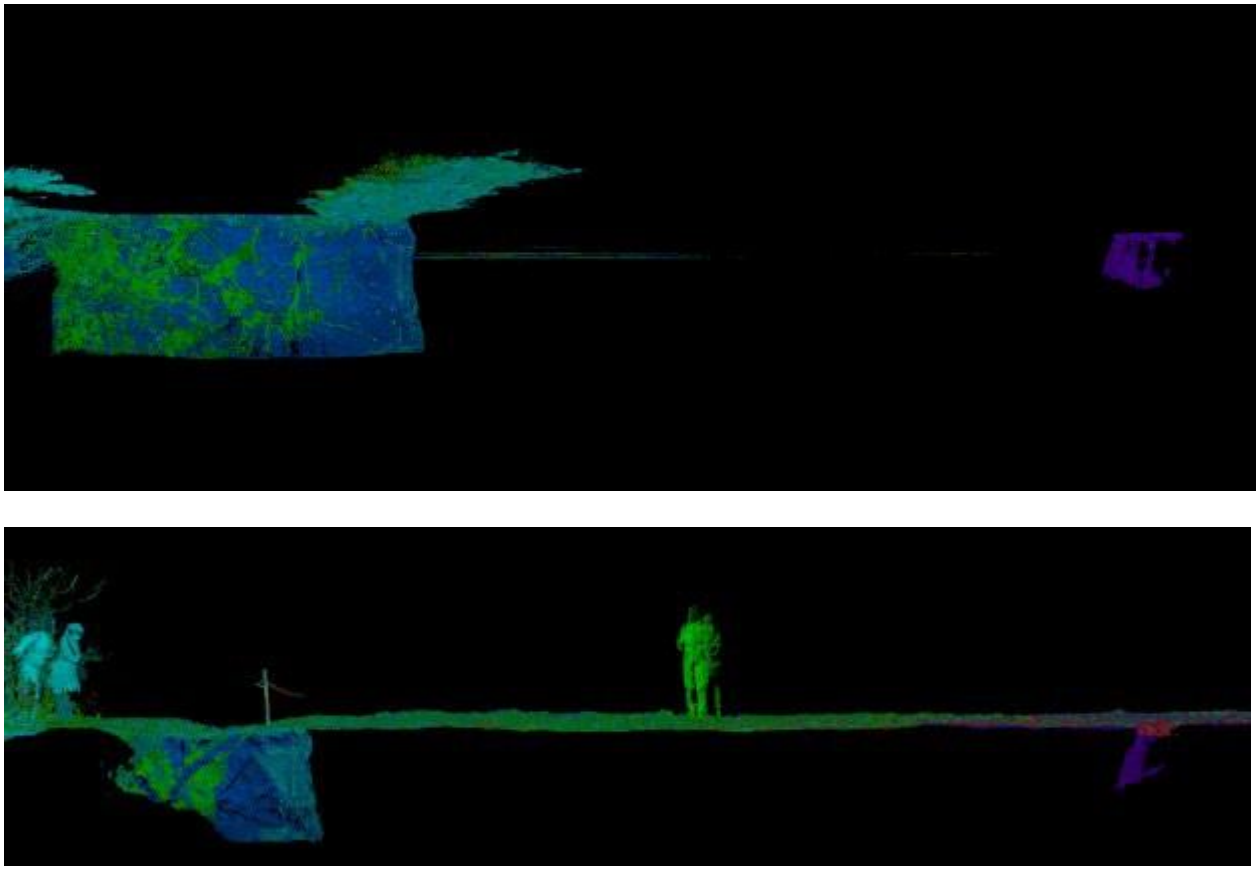

Figure 6.39 Cross-sections of the lidar bundle with two adjacent sinkholes, S007 (45.296599N, 16.415005E) and S008 (45.296589N, 16.415085E).

Figure 6.40 Cross-section of the lidar bundle with two adjacent sinkholes, S023 (45.294192N, 16.416487E) and S024 (45.294139N, 16.416563E).

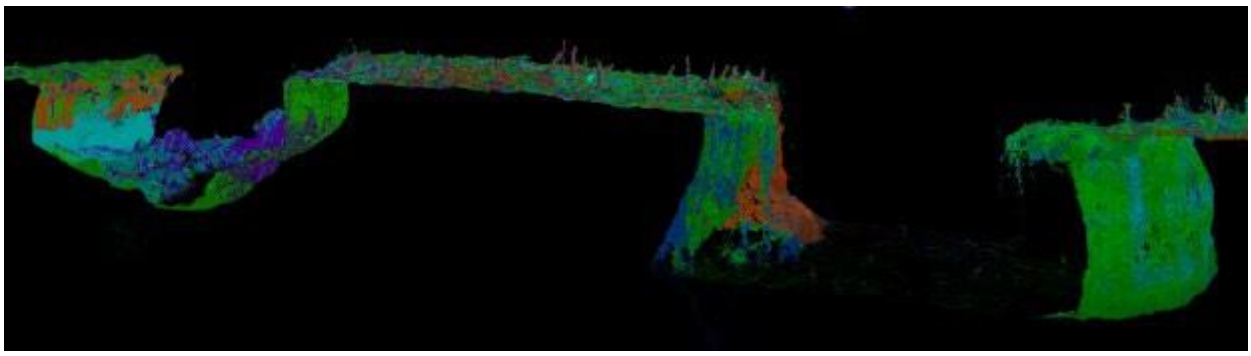

Figure 6.41 Cross-section of the lidar bundle with two adjacent sinkholes, S023 (45.294192N, 16.416487E) and S024 (45.294139N, 16.416563E).

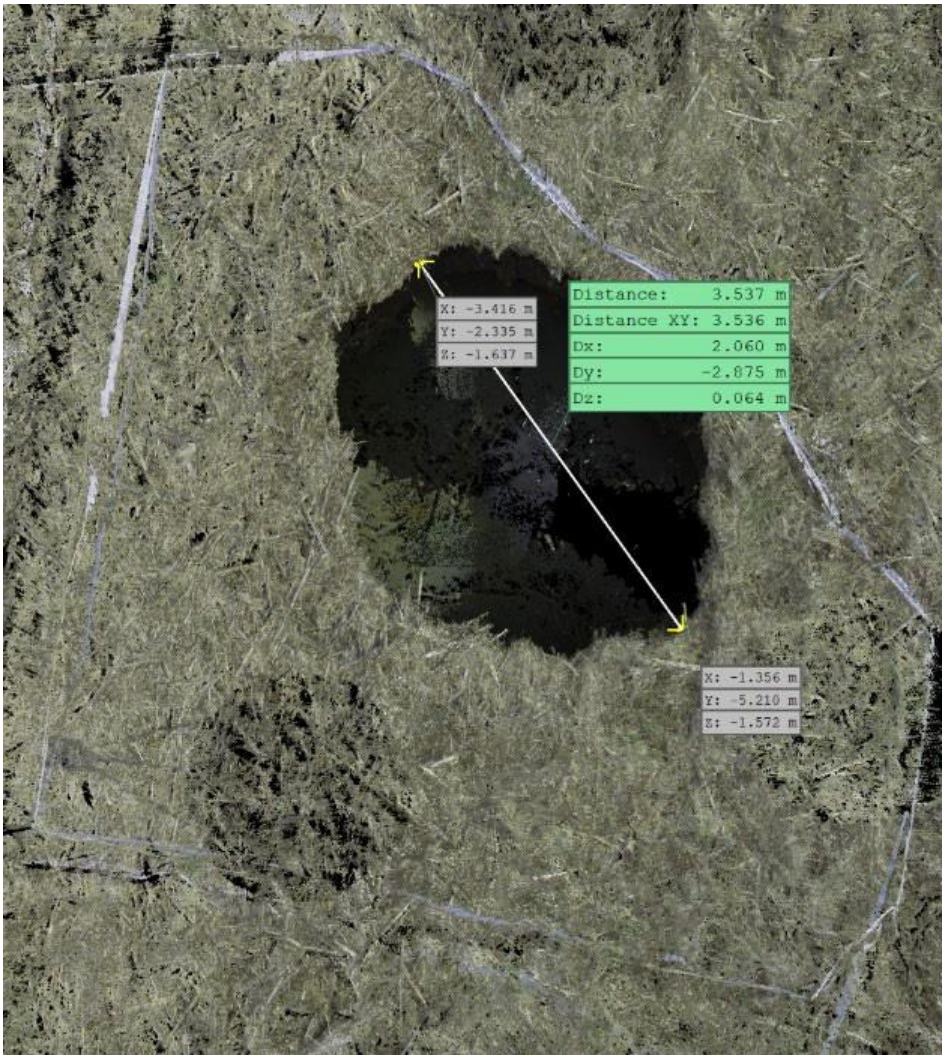

Figure 6.42 The lidar scan of the sinkhole S025 (45.293997N, 16.417133E).

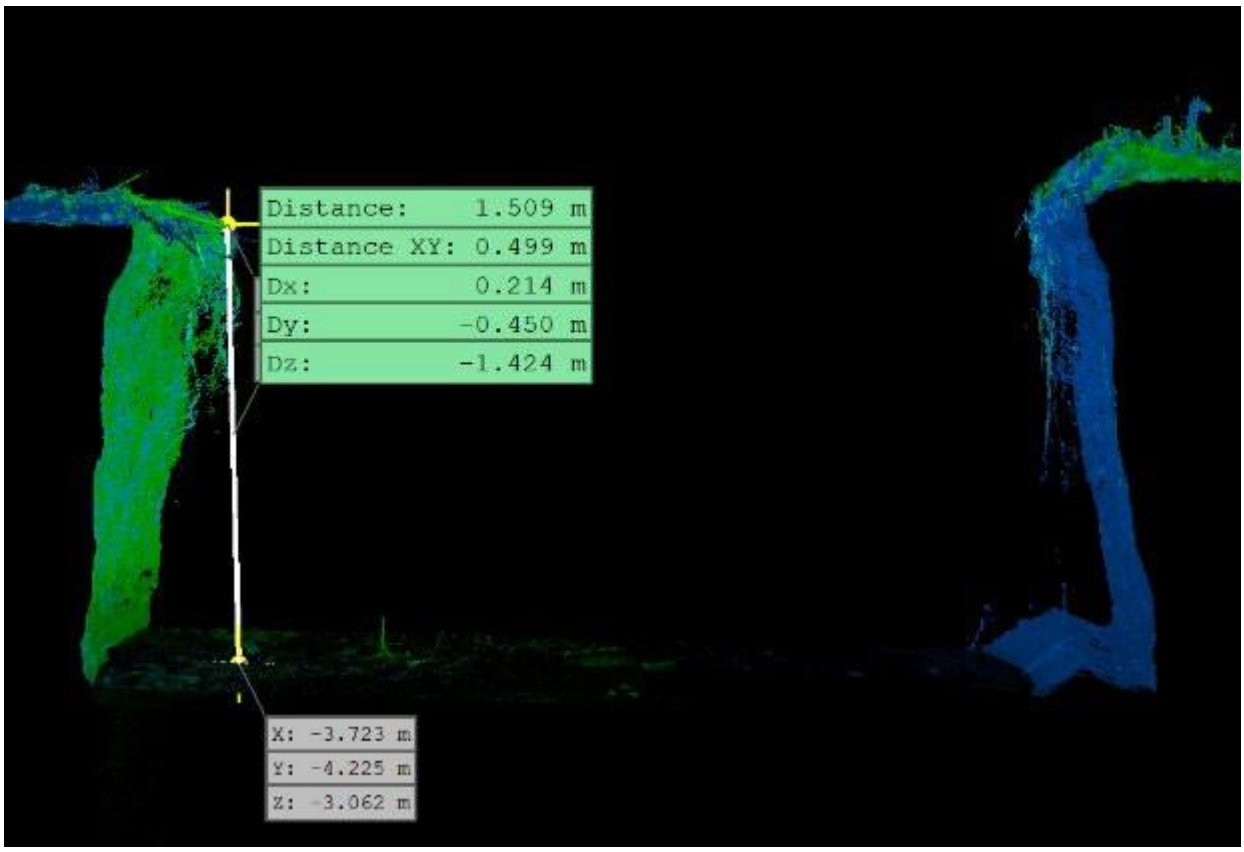

Figure 6.43 The lidar scan with the cross-section of the sinkhole S025 (45.293997N, 16.417133E).

Figure 6.44 The lidar plan view of the sinkhole S043 (45.292195N, 16.422607E).

Figure 6.45 The lidar scan with the cross-section of the sinkhole S043 (45.292195N, 16.422607E).

6.6. Concluding Remarks and Future Work

The GEER reconnaissance team recorded a total of 139 sinkholes surrounding Borojevići and Mečenčani. Although naturally prone to the formation of cover-collapse sinkholes, the area exhibited unusual activity during the Petrinja M6.4 earthquake in December 2020 and aftershocks. The collapsed activity ceased approximately three months after the main shock but is expected to continue in the future with much lower frequency. None of the sinkholes, to our knowledge, synchronously opened at the time of an earthquake, and the time-lag of collapses of several hours or days following the major earthquakes is typical for this site. The area of approximately 4 km^2 is in the alluvial valley between karstic hillslopes and the Sunja river. Repeatability and regularity of cover-collapse sinkholes appearance exist to some extent. For example, relatively smaller, shallower, and closer to each other are sinkholes north of Borojevići and closer to Sunja. More sparsely spatially located, deeper and larger sinkholes collapsed around Mečenčani. Sinkholes are characterized with a few specific features found in almost all cases: vertical or even over hanged sidewalls, and collapsed materials are clays and clayey gravels, which are most likely not overconsolidated, but phase relationship-based calculations using geotechnical indices of samples near S001 sinkhole indicate unsaturated zone. Therefore, we conclude that soil failure is a brittle failure. What remains unknown is the mechanism of collapse, the undefined role of time and seismic load, as well as hydrology and seismicity-related pore pressure fluctuations as possible triggers.

Finally, to put the sinkhole's collapse unusual coseismic activity in context, the GEER virtual team performed a focused literature review on sinkhole occurrence related to earthquakes, given as follows. The 2012 Varzeghan–Ahar earthquake in Iran provided an example of sinkholes opening in response to earthquakes. Two sinkholes were recorded, the first on a riverbed with a diameter of approximately 2 m. The other about 10 m in diameter, but it was noted that cracks developed nearly 15 m from the site. As written in the paper by Memarian and Mahdavifar (2012), "*the area is underlain by a wide variety of sedimentary and volcanic rocks and unconsolidated sedimentary deposits*", diverse in their composition and degree of consolidation, and among which alluvium has been identified. Agreably, Singh et al. (1997) concluded that "*earthquakes* [...] *increase the frequency of the occurrence of sinkholes*". By explaining the increase of pore pressure during the rainy season, Singh et al. are laying the groundwork to understand why there would be 15–20 reported sinkholes every year in the Tohoku district of Japan between 1974 and 1987, "except in 1978 when an earthquake of 7.4 magnitude caused 219 sinkholes". Caramanna et al. (2008) have found that in Southern Italy, "*another group of collapses in plain areas is characterized by thick alluvial or pyroclastic cover over deep-buried bedrock with an upward migration of the phenomenon*," finding the commonality of alluvium near the sinkhole site again. Between the Molise, Basilicata, and Calabria regions of Italy, Caramanna et al. (2008) report that due to soil liquefaction, sinkholes are often isolated and collapse as quickly as 24 hours after a high magnitude earthquake, but rarely beyond 30 days.

In contrast to the previous reports of sinkholes opening after earthquake activity, Chiaro et al. (2015) have studied sinkhole formation since 2013, pointing out earthquakes as a factor that may increase and more severe sinkhole development. They specifically cite the Gorkha earthquake of

2015, during which "*muddy water*" was observed near the event site. Though they did not observe any sinkhole formation because of this earthquake, Chiaro et al. (2015) warned that sinkholes should be anticipated in the future since the water build-up betrays the erosion occurring in the subsoil. These articles clarify that earthquakes can cause sinkhole formation, but certain conditions (soil composition, erosion, pore pressure, water presence) significantly increase the likelihood of sinkhole development.

References

Caramanna, Ciotoli G. and Nisio S. (2008) *A review of natural sinkhole phenomena in Italian plain areas*. Natural Hazards, (45), p145–172. Available at: DOI: https://doi.org/10.1007/s11069-007-9165-7. (Accessed: 8 May 2021)

Chiaro, G., Kiyota, T., Pokhrel, M. R., Goda, K., Katagiri, T. Sharma, K. (2015). *Reconnaissance report on geotechnical and structural damage caused by the 2015 Gorkha Earthquake, Nepal*. Soils and Foundations, 55(5), p.1030-1043. Available at: DOI: https://doi.org/10.1016/j.sandf.2015.09.006

Croatian Seismologic Survey (2021). *Preliminary results of the Petrinja earthquake series between December 28 2020 and January 28, 2021. In Croatian: Preliminarni rezultati serije potresa kod Petrinje od 28. prosinca 2020 do 28. siječnja 2021.* University of Zagreb, Faculty of Science, Department of Geophysics. [Online]. Available at: http://www.pmf.unizg.hr/geof/seizmoloska_sluzba/mjesec_dana_od_glavnog_petrinjskog_potresa#) (Accessed: 8 May 2021)

Gutiérrez F. and Cooper, A.H. (2013). *Surface morphology of gypsum karst*. In: Shroder, J. Treatise on Geomorphology. Karst Geomorphology (6), p425–437. Available at: http://www.speleogenesis.info/directory/karstbase/publication.php?id=13244. (Accessed: 8 May 2021)

Memarian P. and Mahdavifar M. (2012). *Distribution and characteristics of landslides induced by the Varzeghan-Ahar earthquake doublet (Mw=6.4 and Mw=6.3) in 2012 in Azerbaijan Sharghi, northwest of Iran*. In: Proceedings of the *IPL Symposium*. Kyoto, Japan 20-23 November 2012. International Consortium of Landslides.

Singh, K. B. and Dhar, B. B. (1997). *Sinkhole subsidence due to mining*. Geotechnical and Geological Engineering (15) p327-341

Šikić, K. (2014). *Osnovna geološka karta SFRJ 1:100.000, List Bosanski Novi L33-105*. – Fond stručne dokumentacije Instituta za geološka istraživanja, Zagreb. (manuskript) Geologic map available on request at https://www.hgi-cgs.hr/osnovna-geoloska-karta-republike-hrvatske-1100-000/. (Accessed: 8 March 2021)

Vidić M. (2021). *Look how a whole is widening in Mečenčani! Suffusion and karstification of limestone. In Croatian: Pogledajte kako se širi rupa u Mečenčanima! Sufozija i okršavanje*

vapnenačke stijene [Online video] 9 January 2001. Dnevno.hr. Available at: https://www.youtube.com/watch?v=br-ocSaXlDg (Accessed: 15 April 2021)